AD-A021 943

AMOS (ARPA MAUI OPTICAL STATION) SEEING QUALITY
MEASUREMENTS

Darryl P. Greenwood, et al

Rome Air Development Center

Prepared for:

Defense Advanced Research Projects Agency

January 1976

REPORT DOCUMENTATION PAGE		READ INSTRUCTIONS BEFORE COMPLETING FORM
1 REPORT NUMBER RADC-TR-75-295	2 GOVT ACCESSION NO.	3 RECIPIENT'S CATALOG NUMBER
4 TITLE (and Subtitle) AMOS SEEING QUALITY MEASUREMENTS		5 TYPE OF REPORT & PERIOD COVERED In-House Technical Report
		6 PERFORMING ORG REPORT NUMBER ARPA Order Number 2646
7 AUTHOR(s) Darryl P. Greenwood RADC Jim Newman AFCRL Donald O. Tarazano RADC Paul F. Kellen AERL Duane A. Haugen AFCRL Merlin G. Miller AERL J. Chandran Kaimal AFCRL		8 CONTRACT OR GRANT NUMBER(s) N/A
9 PERFORMING ORGANIZATION NAME AND ADDRESS Rome Air Development Center (OCSE) Griffiss AFB NY 13441		10 PROGRAM ELEMENT PROJECT, TASK AREA & WORK UNIT NUMBERS Program Code Number 5E20 Program Element 62301E Job Order No. 26460117
11 CONTROLLING OFFICE NAME AND ADDRESS Defense Advanced Research Projects Agency 1400 Wilson Blvd Arlington VA 22209		12 REPORT DATE January 1976
		13 NUMBER OF PAGES 80
14 MONITORING AGENCY NAME & ADDRESS(if different from Controlling Office) Rome Air Development Center (OCSE) Griffiss AFB NY 13441		15 SECURITY CLASS. (of this report) UNCLASSIFIED
		15a DECLASSIFICATION DOWNGRADING SCHEDULE N/A

16 DISTRIBUTION STATEMENT (of this Report)

Approved for public release; distribution unlimited.

17 DISTRIBUTION STATEMENT (of the abstract entered in Block 20, if different from Report)

Same

18 SUPPLEMENTARY NOTES

Address for AFCRL: Address for AERL:
AFCRL (LYB)   AVCO Everett Research Laboratory
Hanscom AFB MA 01731   2385 Revere Beach Parkway
                           Everett MA 02149

19 KEY WORDS (Continue on reverse side if necessary and identify by block number)

Atmospheric Turbulence   Observatories
Propagation   Acoustic Sounder
Seeing Quality

20 ABSTRACT (Continue on reverse side if necessary and identify by block number)

During the month of August 1974, a series of experiments was conducted at the
ARPA Maui Optical Station (AMOS) on Mt. Haleakala, Maui, Hawaii. The objectives
were to quantify astronomical seeing conditions, and to determine if the seeing
quality has been degraded by the presence of the site structures. Instruments
used were an acoustic sounder (to probe the altitudes of 100 to 1000 ft), fine-
wire microthermal probes (to measure local turbulence in and around the domes)
and a Hartmann sensor (to provide integrated strengths of turbulence for the

DD $_{1\ JAN\ 73}^{FORM}$ 1473   EDITION OF 1 NOV 65 IS OBSOLETE

entire atmosphere). According to fine-wire probe data, local turbulence can be on occasion a significant factor in degrading seeing. These sensors noted some thermal contamination from one of the domes which was in a nearly operational configuration. The acoustic sounder indicated that the strengths of turbulence in 100 to 1000 ft altitude are not sufficient to degrade seeing. Finally, the Hartmann device recorded significantly more degradation than was seen by either of the other two probes. Hence we speculate that there is significant turbulence at high altitude temperature inversions such as at the tropopause.

ACKNOWLEDGMENTS

TABLE OF CONTENTS

TABLE OF CONTENTS (continued)

LIST OF FIGURES

LIST OF TABLES

I.   INTRODUCTION

A.   Background.

The Strategic Technology Office of the Defense Advanced
Research Projects Agency (ARPA) is presently pursuing an ad-
vanced technology program aimed at developing techniques for ob-
taining high resolution images of space objects. The prime goal
is the development of a compensated imaging system which will
sense the effect atmospheric turbulence has on images and correct
for the phase aberrations in realtime. For the proper design
of such a system, ARPA needed an objective quantification of
seeing quality at their prime optical site AMOS (ARPA Maui Opti-
cal Station, located in Maui, Hawaii). An equally important goal
was to determine if the seeing quality had been degraded by the
presence of the site structures and therefore if it could be
improved by certain modifications.

The AMOS facility, shown in the photographs of Figs. 1
and 2, is comprised of two main observation domes, one contain-
ing twin 48 inch telescopes and the other a 60 inch telescope.
A third dome shown in the figure was not present during the
experiments which we will describe.

The basis for the concern that seeing quality may have
been reduced by the presence of the buildings is a series of
measurements taken during the initial site survey.[1] The measure-
ments indicated that seeing was often better than 0.4 arc sec

1

Figure 1. Aerial View of the Summit of Mt. Haleakala, taken roughly to the ENE, looking into crater. AMOS is at the left in this photograph.

2
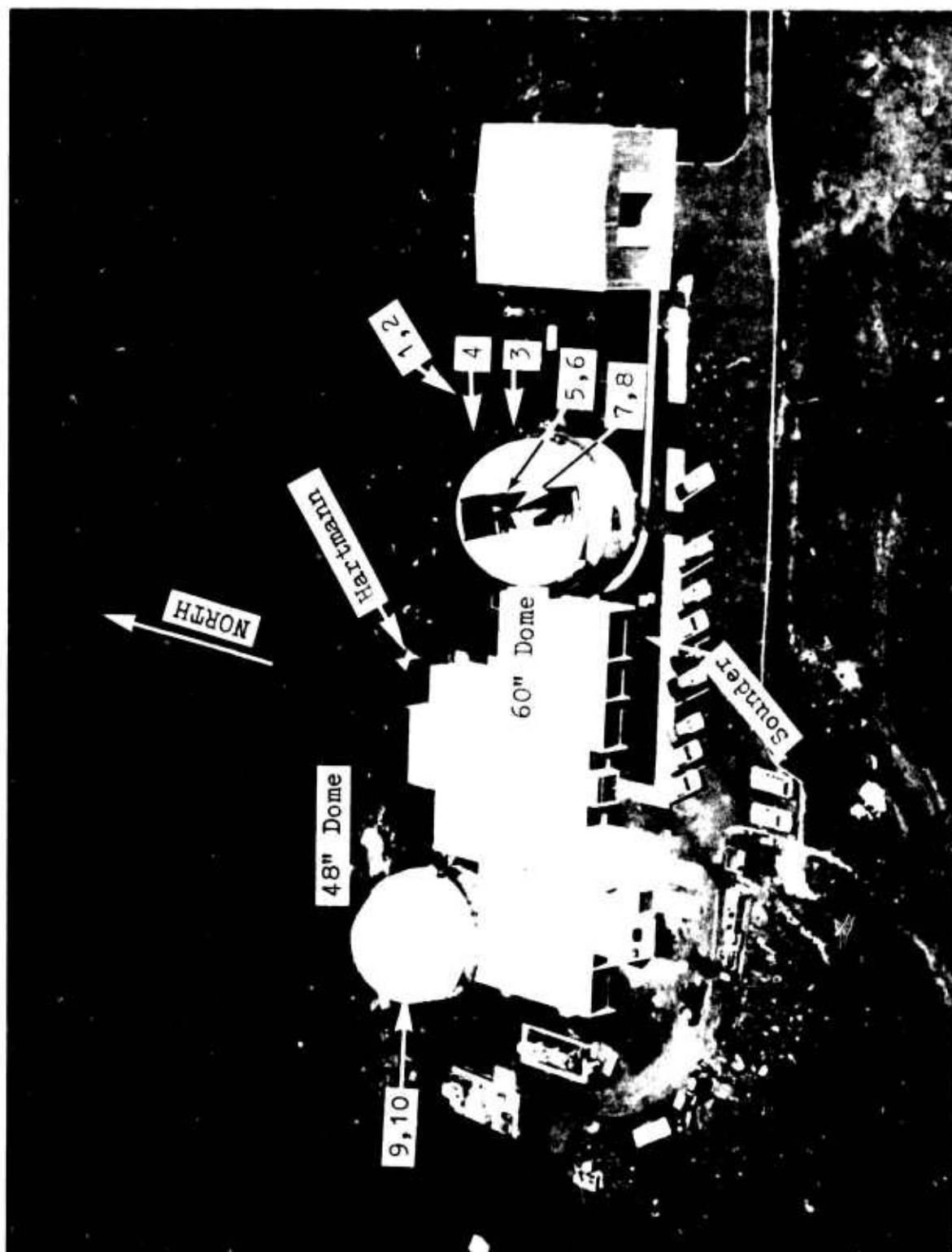
Figure 2. Aerial View of AMOS, showing location of sensors used in this experiment. Note the Acoustic Sounder and Hartmann devices are not present in this photograph.

3

and actually approached 0.1 arc sec at times. The confusing factor is that the telescope used was 12.5 inches in diameter. Thus the values should not be less than the Rayleigh resolution limit, 1.22 λ/D (where λ = wavelength and D = diameter) which is 0.4 arc sec. Scientists using the observatory have stated that a subjective seeing limit which they observe is approximately 1 arc sec. We may either conclude there were errors in the original survey or that the dome structures did degrade the seeing.

B. Experimental Plan.

To pursue the objective of quantifying seeing at AMOS, the Environmental Studies Section of the Rome Air Development Center formed an experimental team consisting of their own personnel as well as those of the Boundary Layer Branch of Air Force Cambridge Research Lab (AFCRL) and AVCO Everett Research Lab (AERL). The three organizations collaborated on the formulation of the experimental plan, as well as the content of this report. The plan called for measurements of local turbulence with an acoustic sounder and fast-response microthermal probes. To determine the percentage contribution of the local effects, a measure of integrated turbulence for the whole atmosphere was to be measured with a Hartmann sensor. Data were to be taken both inside and outside the domes to determine the influence of the dome structures. Only the acoustic sounder was to operate at a fixed location, and it would provide turbulence profiles in

4

the altitudes of 100 to 1000 ft.

The series of experiments were run at AMOS during August 1974. RADC provided the acoustic sounder and microthermal probes and personnel to operate the microthermal devices. AFChL provided data recording equipment, a Lyman-alpha humidiometer and a wind set, but most importantly provided scientific guidance for the experiments. AFCRL also operated the sounder as a prelude to their full calibration experiments to be undertaken just two months later. Personnel from AERL assembled the optical sensor and were responsible for its operation.

C. General Conclusions.

Rather than to keep the reader in suspense, we will briefly summarize our most important conclusions:

(1) Although scientifically interesting activity was noted by the sounder in the range of 100-1000 ft, it was not of sufficient strength to degrade seeing.

(2) Turbulence in and around the dome structures can on occasion be a significant factor in degrading seeing.

(3) Local turbulence appears to be naturally generated in most instances, but the data are too limited to be certain. (Hence on this basis we still can not say if the original site survey data were faulty.)

(4) Additional seeing degradation is caused by thermal

5

contamination within the 48 inch dome.

(5) The remaining turbulence not sensed by the sounder and fine wire probes, yet sensed by the Hartmann device, must be above 1000 ft or in the range of 60 to 100 ft. Thus tropopause turbulence is probably significant.

II. TURBULENCE MEASUREMENTS

A. Experimental Design.

Sharp gradients in refractive index of air cause re-
fraction and scattering of light rays. Spatial and temporal
variations in these gradients are responsible generally for limi-
tations in seeing quality, or resolution, with any given tele-
scope. Fluctuations in the refractive index, in turn, are
strongly dependent on temperature fluctuations and, to a lesser
degree, on moisture fluctuations. Primary emphasis in these
experiments was therefore on measuring temperature fluctuations.
Up to ten microthermal sensors especially designed for measuring
small scale temperature fluctuations[4,5] were deployed at various
positions in and around the dome. The actual positions of these
sensors are listed in Table 1 and depicted in the photograph of
Fig. 2. In addition to these sensors, an acoustic sounder mea-
suring echoes from temperature discontinuities up to a height of
1000 feet was used. The sounder was specially procured from the
Wave Propagation Laboratory, NOAA, by RADC for use in studies of
this type. Details of the acoustic sounder as an instrument for
probing temperature structure may be found in a recent WPL
report.[6] It is suffice to note here that the sounder was operated
in a mode to provide usable data between heights of roughly 100
and 1000 feet.

Wind speed and direction were measured with a cup

7

TABLE 1

Position of Microthermal Sensors for August 1974 AMOS Experiments

Position No.	Location
1, 2	4 m above ground, 12 m NNE of 60" dome foundation, probes 1 (left) and 2 (right), separated by 0.76 m.
3	8.4 m above ground, 3 m NE of 60" dome foundation.
4	15.6 m above ground, 3 m NE of 60" dome foundation.
5	Approximately 1.5 m inside 60" dome surface, 8 m above dome floor.
6	Approximately 1.5 m outside 60" dome surface, 8 m above dome floor.
7	Inside 60" telescope tube, at base of tube.
8	Inside 60" telescope tube, at top of tube.
9	Approximately 1.5 m inside 48" dome surface, 8 m above dome floor.
10	Approximately 1.5 m outside 48" dome surface, 8 m above dome floor.

anemometer and a wind vane to permit relating speed and direction to the orientation of the dome slot. Moisture fluctuations were also measured with a Lyman-alpha humidiometer for a few runs to obtain preliminary data on their importance to refractive index fluctuations at AMOS. No processing of the microhumidity data was done, as it was obvious from observing the signal levels that there was insignificant humidity turbulence.

All the data were recorded on a 14-channel analog tape recorder for subsequent analysis. In addition, the acoustic sounder return was recorded on a facsimile chart as a function of time and height to provide an immediate graphic record of the spatial and temporal variations in the temperature structure. It should be noted, however, that the facsimile records provide only a qualitative measure of the echo intensity, and the variations in it, since the gain setting for the recorder is always adjusted for optimum contrast and not set at a predetermined level. The sounder data recorded on analog tape were processed at a later time to provide profiles of turbulence with accuracy of typically ± 20%.

B. Data Analysis Procedures for the Fine-Wire Probes.

The temperature data have been digitized at a rate of 10 per second for the length of each observational period, which was normally slightly in excess of three hours. The standard deviation σ_T of the temperature fluctuations was then computed for successive five minute periods. In addition C_T^2, the

9

temperature structure parameter, is computed from microtemperature measured on a pair of probes positioned away from the domes. We then calculate C_T^2 for the remaining sensors for which we have only standard deviations computed. This step is imperative since it is C_T^2 and *not* σ_T which is used in optical propagation calculations.

By definition, C_T^2 is the constant of proportionality in the Kolmogorov inertial subrange form of the temperature structure function:

$$D_T(r) = C_T^2 \, r^{2/3}, \tag{1}$$

where r = separation (traditionally in meters). Since the structure function is the mean square value of the temperature difference for two probes separated a distance r, we may write this simple relation for C_T^2:

$$C_T^2 = \langle (T_1 - T_2)^2 \rangle \, r^{-2/3}, \tag{2}$$

where T_1 and T_2 are temperatures at positions 1 and 2, and the units of C_T^2 are $°C^2 m^{-2/3}$. We may take the brackets $\langle \cdot \rangle$ as representing a time average although strictly speaking they represent an ensemble average. (Hence ergodicity is assumed.)

It is reasonable to expect that the levels of turbulence inside the dome and inside the telescope tube are strongly influenced by wind speed and its direction relative to the orientation of the dome slot. That is, a large amount of turbulent

10

activity inside the dome can be related to turbulence in the atmosphere outside the dome, as well to thermal activity generated inside the dome. Therefore, the average wind speed and direction were computed and tabulated for each run.

Nearly all the observational periods were scheduled between local sunset and sunrise. One three-hour period was scheduled during daytime hours to obtain data during convective mixing situations for comparison purposes. A summary of the data runs completed is given in Table 2. The microtemperature sensor positions which were active for each run are listed here. This table also contains the overall mean wind speed, wind direction, and the dome slot orientation for each run.

C. Conversion of Standard Deviations to C_T^2.

In order to use existing propagation theory, we must insure that the turbulence was Kolmogorov. Figure 3 is a set of sample spectra for Run 16 and covers an 88 minute period. Although this time period is short with respect to the entire experiment and although only three sensors are shown, we have found this to be representative of all the data. Note that the spectra exhibit a nearly $f^{-5/3}$ behavior in the inertial subrange. Hence the turbulence appears Kolmogorov. Also note that the spectra do no flatten into an f^0 power law until very low frequencies. This indicates large values of outer scale, which would be expected at these altitudes.

11

TABLE 2

Summary of August 1974 AMOS experiments

Run No.	Time (HST)	Day	Active Sensor Positions	Wind Speed (m/sec)	Wind Direction	Dome Slot Orientation
3	1835-2145	20	1 thru 4	2	NNW	Not opened
4	1845-2152	21	1 thru 8	4	SE	NE
5	2207-0119	21/22	1 thru 8	7	S	NE
6	0140-0450	22	1 thru 8	7	S	NE
7	1857-2205	22	1 thru 8	3	S	NE
8	2237-0145	22/23	1 thru 8	2	S	NE
9	1913-2022	23	1 thru 8	9	NNE	SW
10	2055-0006	23/24	1 thru 8	2	NNW	
11	0042-0353	24	1 thru 8	missing	NNW	SSW
12	0412-0719	24	1 thru 8	missing	NNW	SSW
13	2110-0020	24/25	1 thru 10	missing	NNE	SSW*
14	0550-0905	25	1 thru 10	4	NNE	NE*
15	2020-2325	25	1 thru 10	6	S	NE*
16	2345-0250	25/26	1 thru 10	6	S	NE*
17	1856-2002	26	1 thru 8	2	S	NE
18	2210-2328	26	1 thru 8	1	S	NE

*The 48" dome slot, instrumented for these four runs, was oriented SSW.
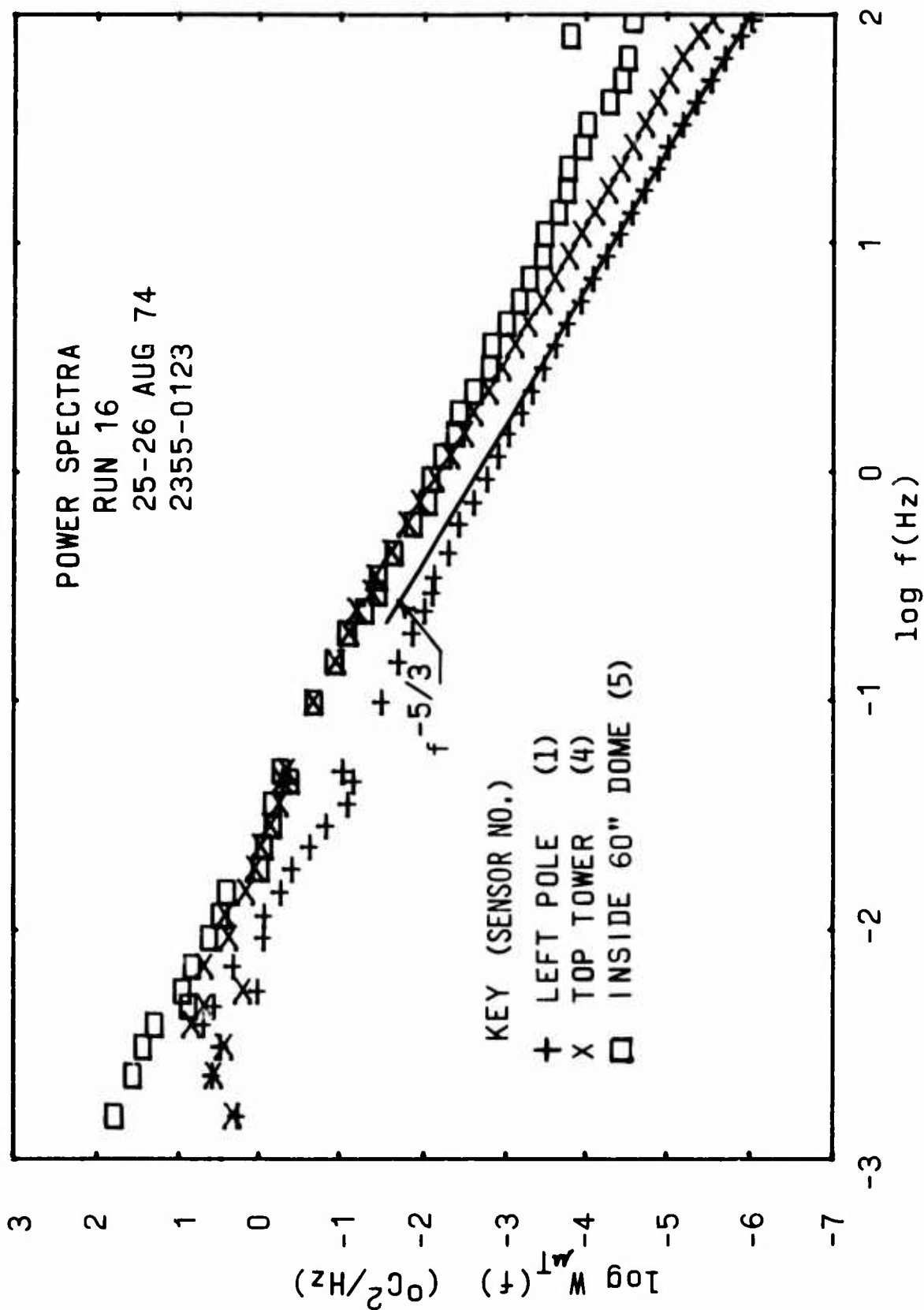
Figure 3. Power Spectra for Run 16 for microthermal sensors 1, 4 and 5.

To convert the standard deviation σ_T at an individual sensor to C_T^2, we use this equation:[4]

$$C_T^2 = 1.91 \ \sigma_T^2 \ L_0^{-2/3}. \tag{3}$$

The additional unknown here is the outer scale L_0 and that is found from the probe pair mounted on the pole north of the dome (sensors 1 and 2). For that pair we know both σ_T^2 (twice, since there are two sensors there) and C_T^2, and thus we know L_0 via Eq. (3). In Fig. 4 we have plotted L_0 for some selective runs over three days. We found that it changed little throughout a mission, as long as the sun neither rose nor set during that mission. For all the nighttime runs, the values of L_0 ranged between 8 and 100 m.

We have encountered much discussion on this procedure of converting σ_T to C_T^2. The argument is basically that the value of L_0 measured at the pole (sensors 1, 2) may not apply at the other sensor locations. First we must remind the reader that we *must* have values of C_T^2 and not σ_T to do the optical propagation computations. Second, we checked very carefully the qualitative behavior of the σ_T plots (versus time) and the C_T^2 plots so derived. We found that we could make exactly the same conclusions based on the C_T^2 plots as we could with the σ_T plots. Third we found that the spectra, such as we show in Fig. 3, indicate large values of outer scale, although not necessarily so large near the dome surface as it is on the pole. Fourth, the values of outer scale as shown in Fig. 4 do not change so rapidly

14
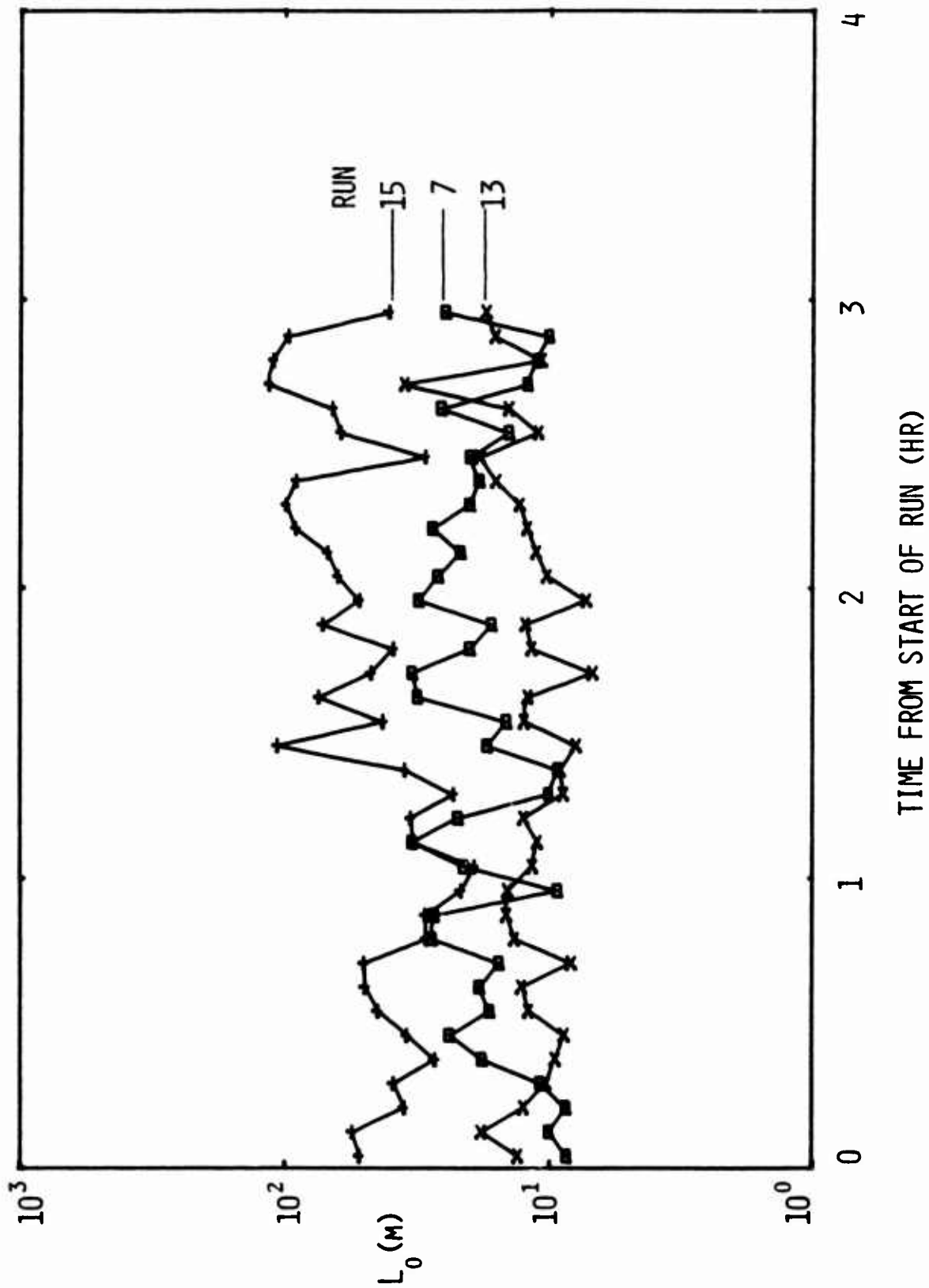
Figure 4. Outer Scale L_0 versus time from start of mission for Runs 7, 13 and 15, on three different nights.

as to give an apparent change in C_T^2 where a change had not
occured in σ_T. Finally, on limited runs we high-pass filtered
the data so that all the sensor signals had the same cut-off
frequency, and we recomputed C_T^2. This method gave values in
good agreement with the method used here. We certainly accept
the argument that the value of L_0 as measured at the pole does
not apply inside the telescope tube, but the signal levels there
were so low as tc almost be in the noise. We will show some
tube data, but it is of very low strength.

D. <u>Discussion of the Qualitative Nature of the Data.</u>

We have plotted values of C_T^2 versus time for those runs and
sensors which we feel are significant. This includes Runs 3,
4, 7, 10, and 12-18. With the exception of Run 3, we have
plotted C_T^2 for sensors 1, 4, 5 and 6. In Runs 14-16 we have
also provided C_T^2 on sensors 6, 9 and 10, thus relating behavior
at the 48" dome to the 60". In addition, for Runs 3, 4, 7, 16
and 17 we have reduced the facsimile plots from the sounder to
a convenient format for comparison with microthermal data. All
of this can be found in Figs. 5-18.

Let us direct our attention first to the facsimile
records. The darkened areas on the records indicate regions
from which back-scattered acoustic energy was received; i.e.,
regions within which fluctuating temperature gradients are suf-
ficiently strong to produce detectable back-scatter. The distri-
bution of these regions in space and time is extremely important

16

Figures 5-18. Plots of C_T^2 and acoustic sounder returns versus time during the mission. (Remaining information on mission and a key are shown in each graph).

Figure 5

18

AMOS RUN 4

21 AUG 74

ACTIVE SENSORS 1-8

WS 4M/SEC

WD SE

60" DOME NE

KEY (POSITION NO.)

——— POLE (1)

– – – TOP TOWER (4)

· · · · · IN SLOT 60" (5)

–·–·– OUT SLOT 60" (6)

Figure 6

19

AMOS RUN 7
22 AUG 74

ACTIVE SENSORS 1-8

WS 3M/SEC
WD S
60" DOME NE

KEY (POSITION NO.)
—— POLE (1)
——— TOP TOWER (4)
······ IN SLOT 60" (5)
—·— OUT SLOT 60" (6)

Figure 7

C_T^2 ($°c_M^2$-2/3)

TIME (HST)

HT(FT)

20

TIME (HST)

$C_T^2 (^{\circ}C^2 M^{-2/3})$
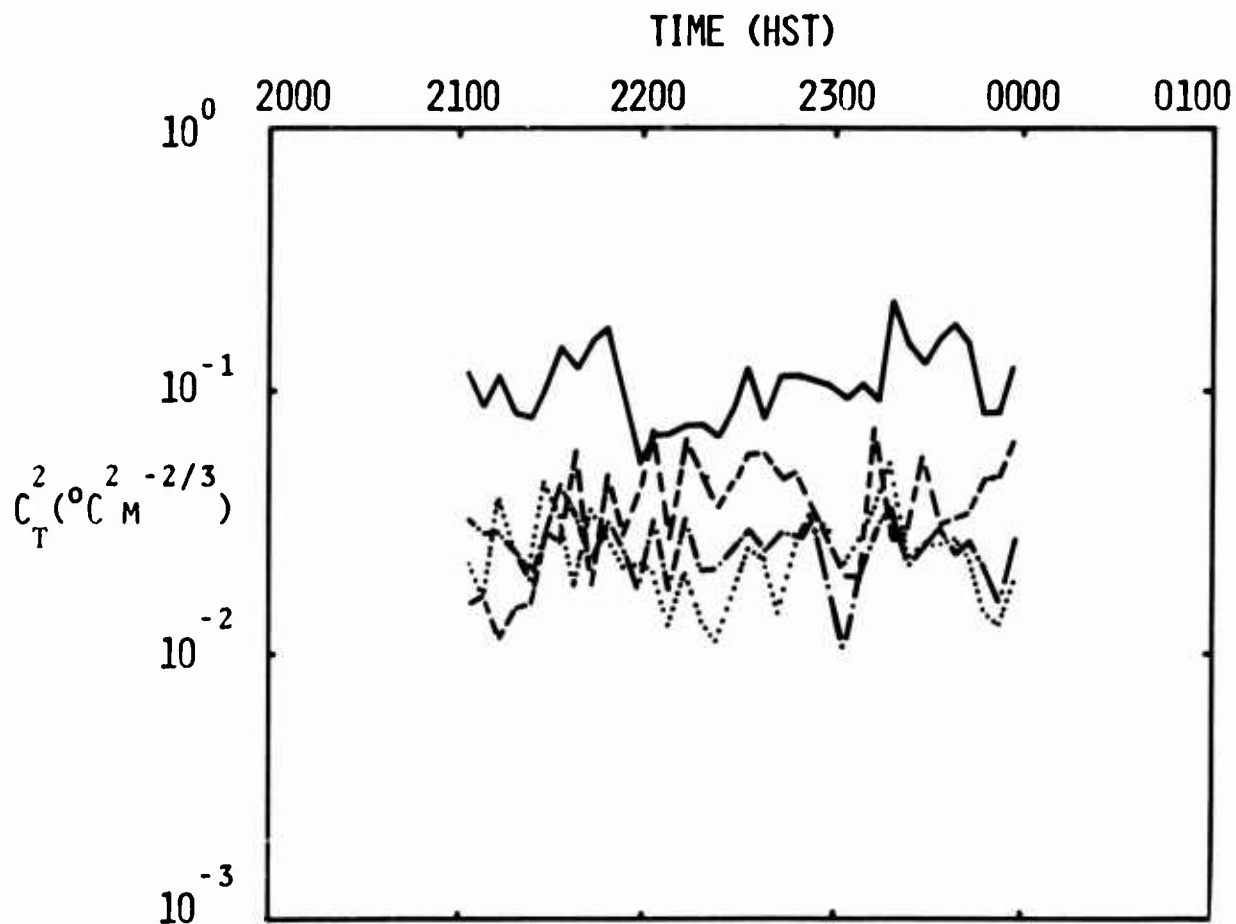
AMOS RUN 10
23-24 AUG 74

ACTIVE SENSORS 1-8

WS 2 M/SEC

WD NNW

KEY (POSITION NO.)
——— POLE (1)
– – – TOP TOWER (4)
········ IN SLOT 60" (5)
—·— OUT SLOT 60" (6)

Figure 8

21

TIME (HST)

$C_T^2 (^{\circ}C^2 M^{-2/3})$
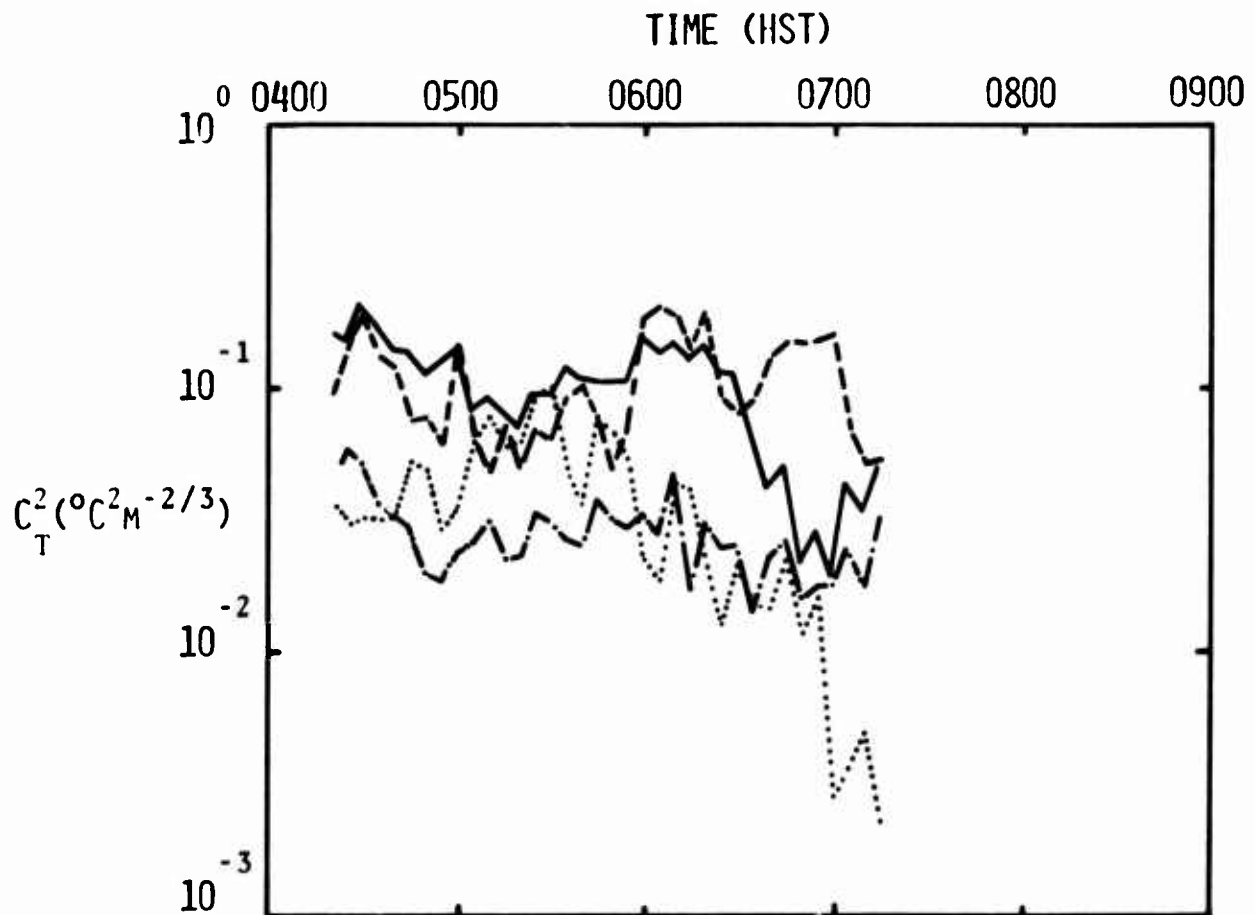
AMOS RUN 12
24 AUG 74

ACTIVE SENSORS 1-8
WS (NOT AVAIL)
WD NNW
60" DOME SSW

KEY (POSITION NO.)
——— POLE (1)
— — — TOP TOWER (4)
·········· IN SLOT 60" (5)
—·— OUT SLOT 60" (6)

Figure 9

22

TIME (HST)

$C_T^2(^{\circ}C^2_M{}^{-2/3})$
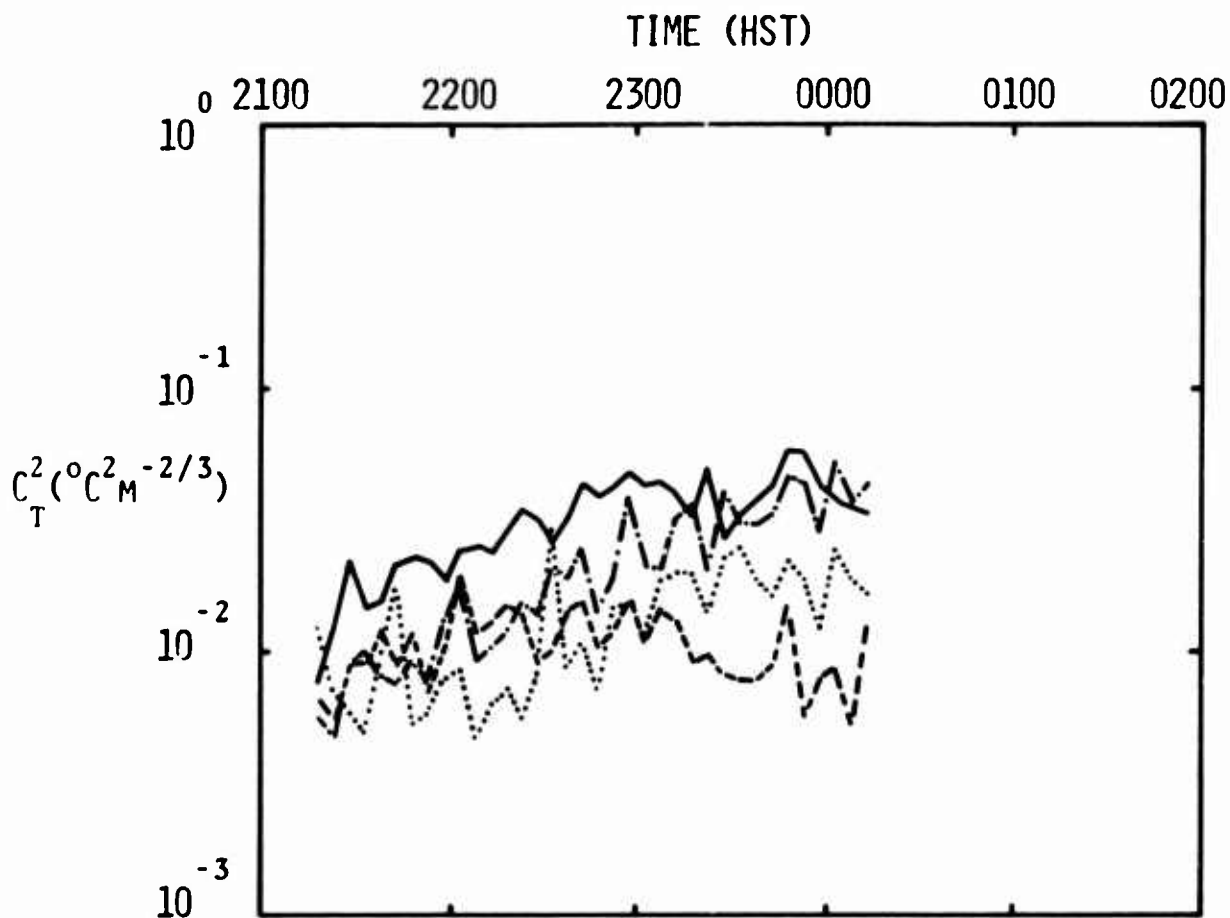
AMOS RUN 13
24-25 AUG 74

ACTIVE SENSORS 1-10
WS (NOT AVAIL)
WD NNE
60" DOME SSW
48" DOME SSW

KEY (POSITION NO.)
——— POLE (1)
— — — TOP TOWER (4)
············ IN SLOT 60" (5)
—·— OUT SLOT 60" (6)

Figure 10

TIME (HST)

C_T^2 $(°C^2_M{}^{-2/3})$

AMOS RUN 14
25 AUG 74

ACTIVE SENSORS 1-10

WS   4M/SEC
WD   NNE
60" DOME   NE
48" DOME   SSW

KEY (POSITION NO.)
——— POLE (1)
— — TOP TOWER (4)
······ IN SLOT 60" (5)
—·— OUT SLOT 60" (6)

Figure 11
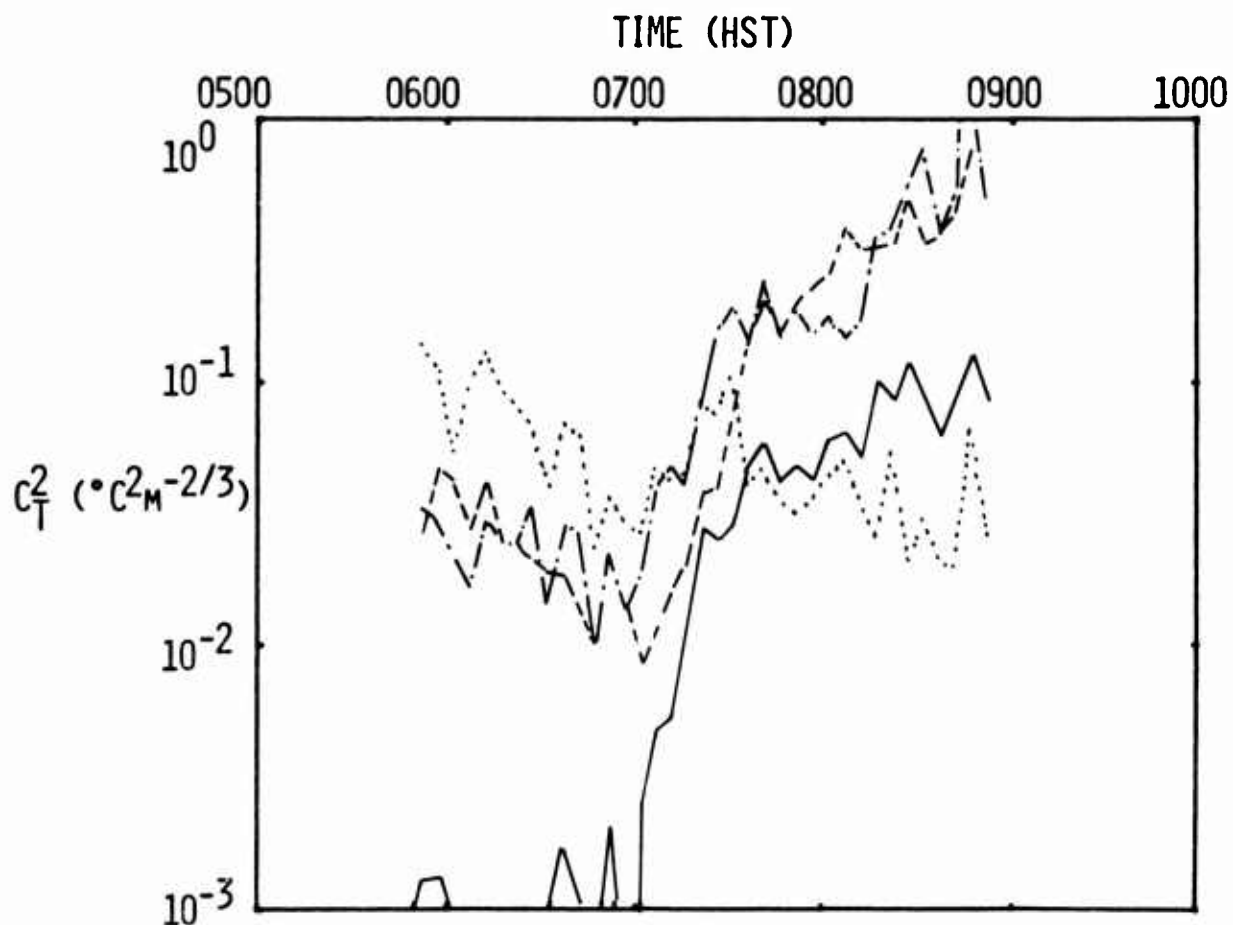
TIME (HST)

C_T^2 $(°C_M^2{}^{-2/3})$

AMOS RUN 14
25 AUG 74

ACTIVE SENSORS 1-10

WS   4m/sec
WD   NNE
60" DOME   NE
48" DOME   SSW

KEY   (POSITION NO.)
———— TOP 60" TUBE (8)
– – –– OUT SLOT 60" (6)
········· IN SLOT 48" (9)
— ·— OUT SLOT 48" (10)

Figure 12

TIME (HST)

C_T^2 ($°C^2 M^{-2/3}$)

15-1 Out   15-2 In
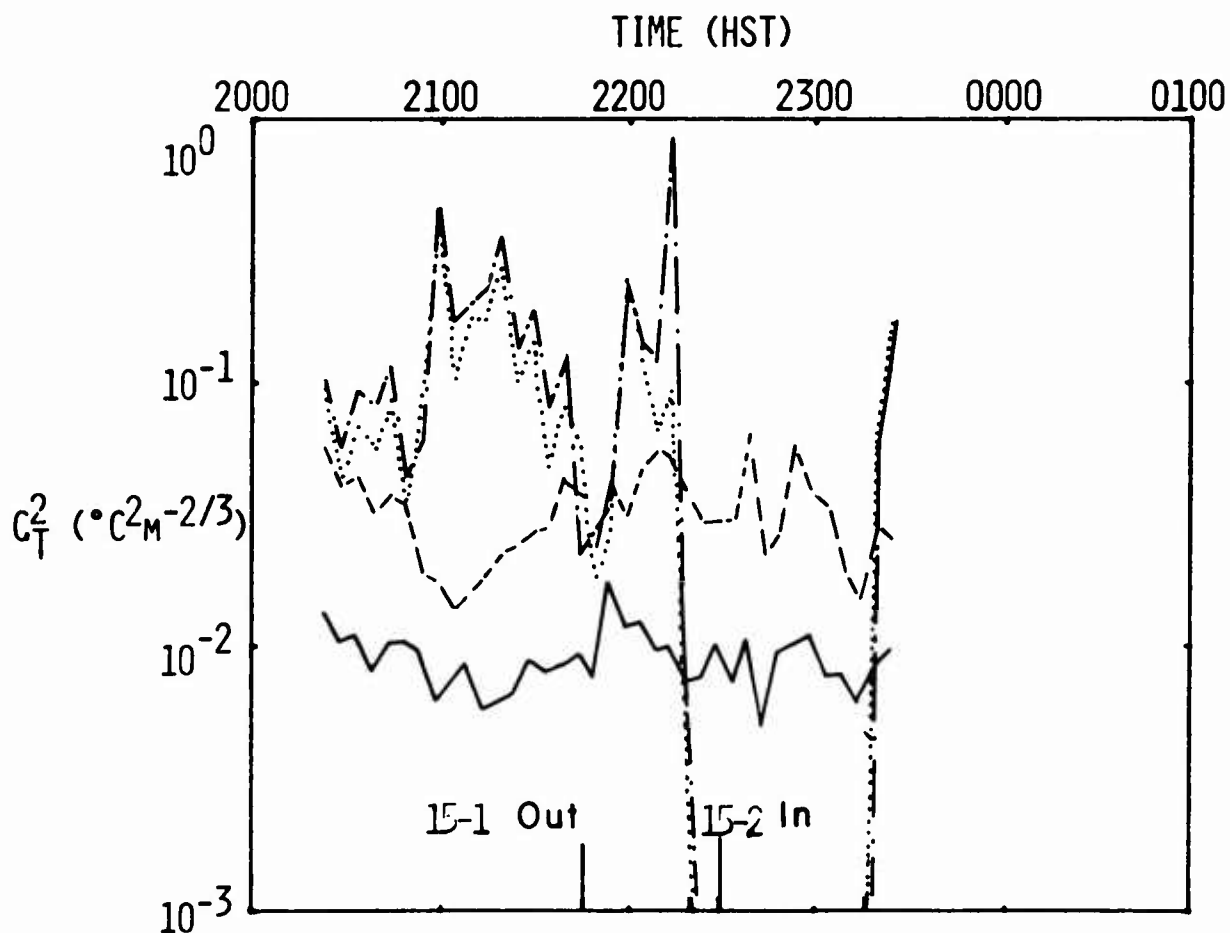
AMOS RUN 15
25-26 AUG 74

ACTIVE SENSORS 1-10

WS 6M/SEC
WD S
60" DOME   NE
48" DOME   SSW

KEY (POSITION NO.)
———   POLE (1)
— — — TOP TOWER (4)
.... IN SLOT 60" (5)
—·—   OUT SLOT 60" (6)

Figure 13

26

TIME (HST)

C_T^2 $(\cdot C^2 M^{-2/3})$

AMOS RUN 15
25-26 AUG 74

ACTIVE SENSORS 1-10

WS 6M/SEC
WD S
60" DOME NE
48" DOME SSW

KEY (POSITION NO.)

———   TOP 60" TUBE   (8)
— — —   OUT SLOT 60"   (6)
......   IN SLOT 48"   (9)
— · —   OUT SLOT 48"   (10)

Figure 14

AMOS RUN 16
25-26 AUG 74

ACTIVE SENSORS 1-10

WS 6M/SEC

WD S

60" DOME NE

48" DOME SSW

KEY (POSITION NO.)

——— POLE (1)

– – – TOP TOWER (4)

······ IN SLOT 60" (5)

—·— OUT SLOT 60" (6)

1000

HT(FT)

100

TIME (HST)

2300   0000   0100   0200   0300   0400

10^0

10^{-1}

C_T^2 $(°C^2_M{}^{-2/3})$

10^{-2}

10^{-3}

16-1 In 16-2 Out

28

Figure 16

29
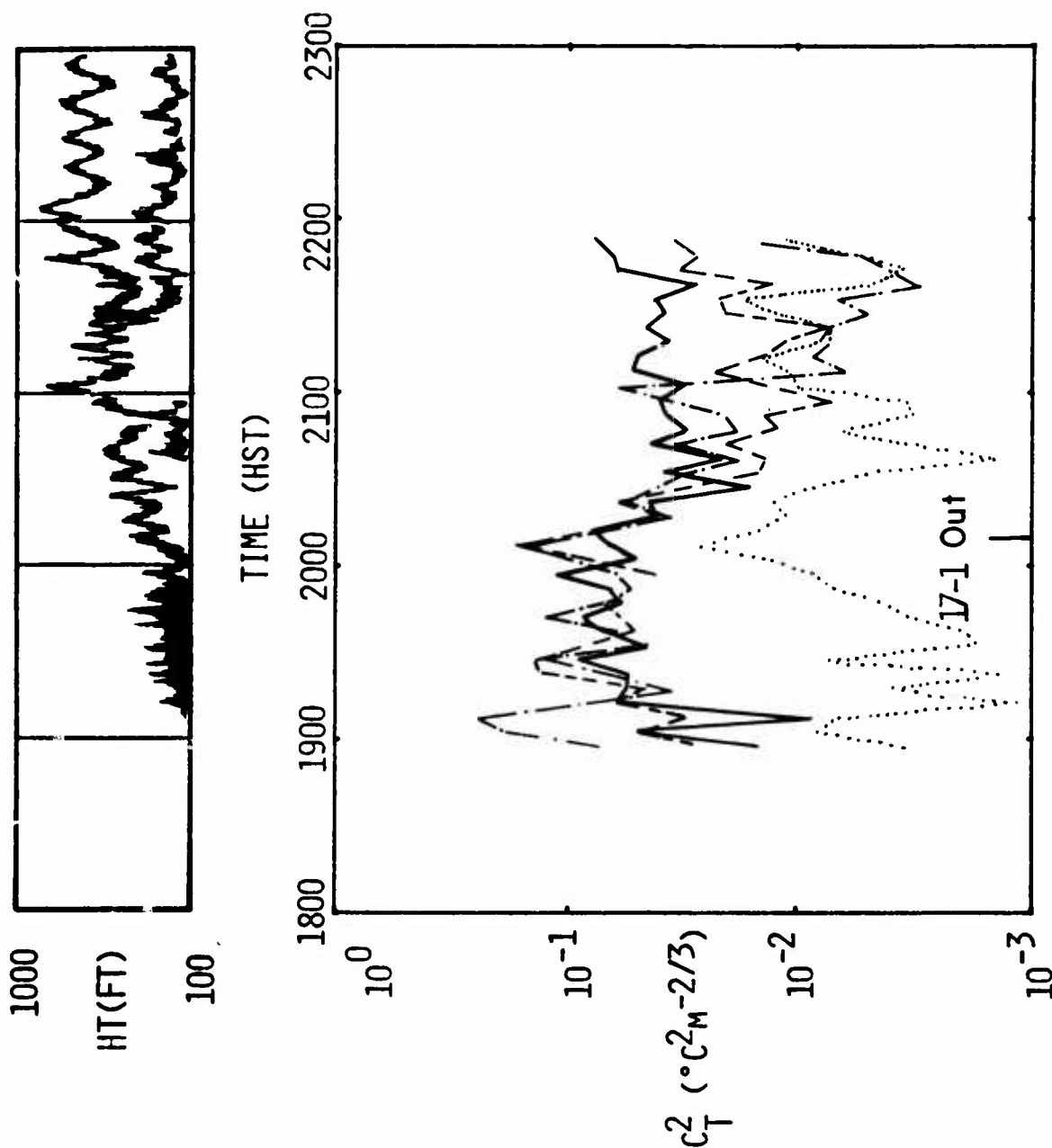
AMOS RUN 17

26 AUG 74

ACTIVE SENSORS 1-8

WS 2m/sec

WD S

60" DOME NE

KEY (POSITION NO.)
——— POLE (1)
——— TOP TOWER (4)
·········· IN SLOT 60" (5)
—·—·— OUT SLOT 60" (6)

TIME (HST)

HT(FT)

C_T^2 ($\cdot C^2_M$−2/3)

17-1 Out

1000

100

1800   1900   2000   2100   2200   2300

10^0
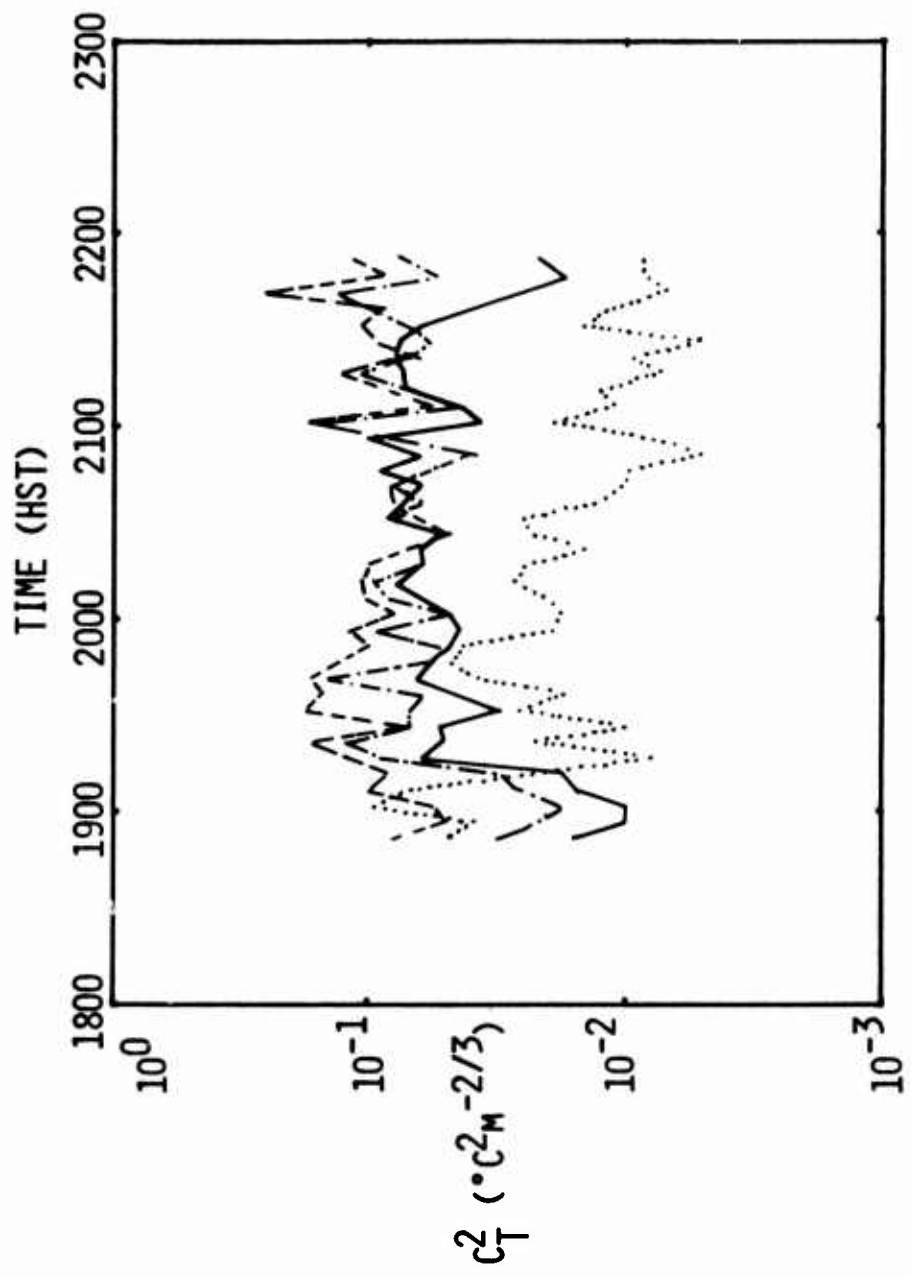
10^{-1}

10^{-2}

10^{-3}

Figure 17
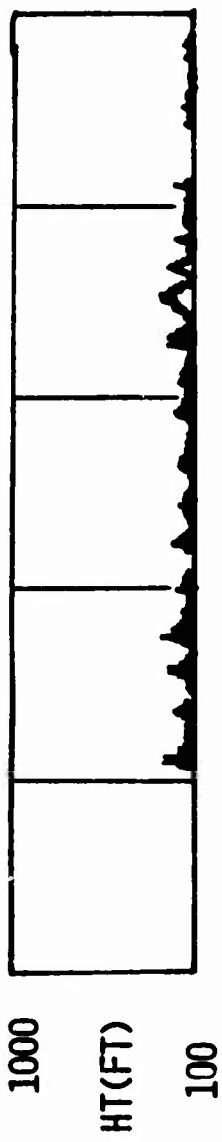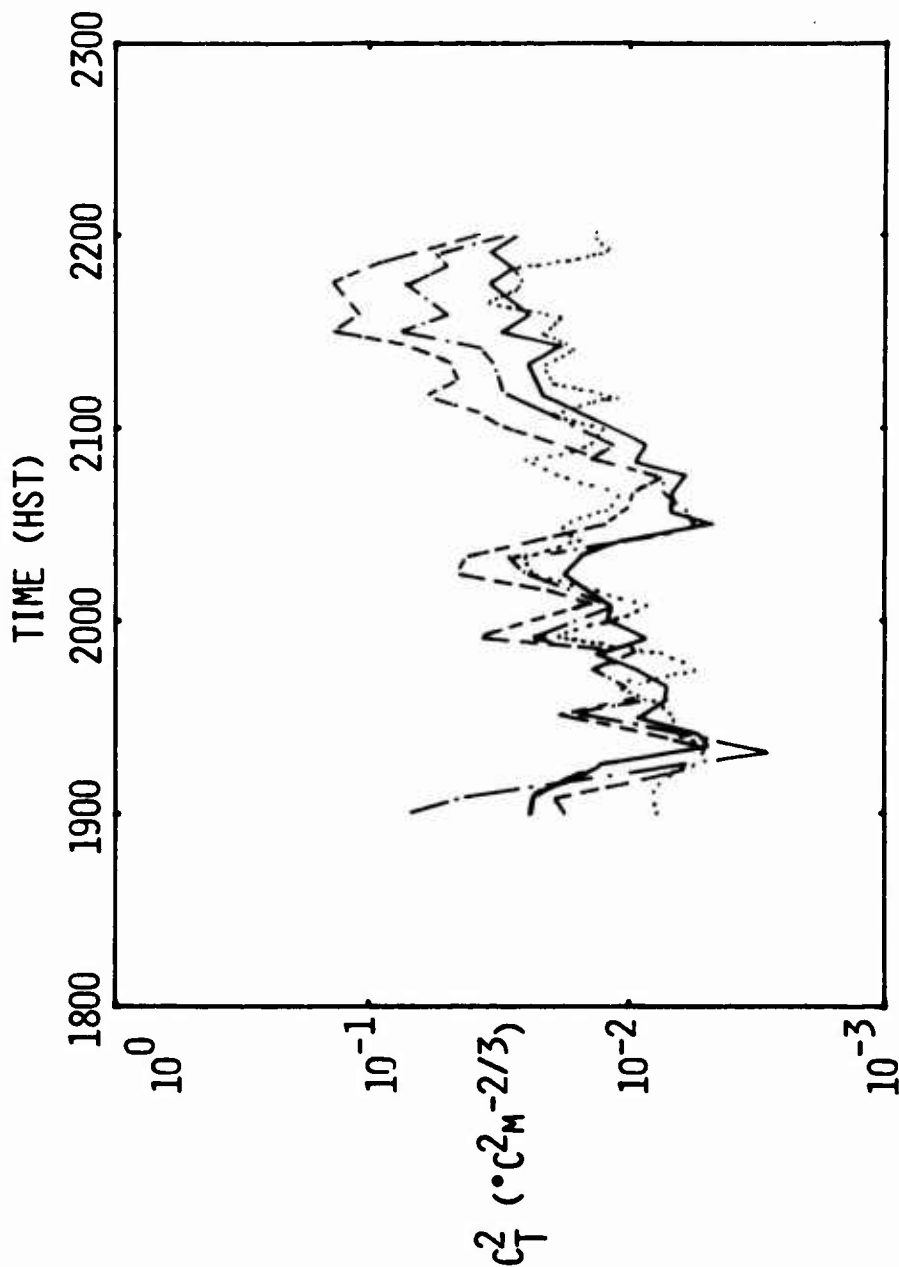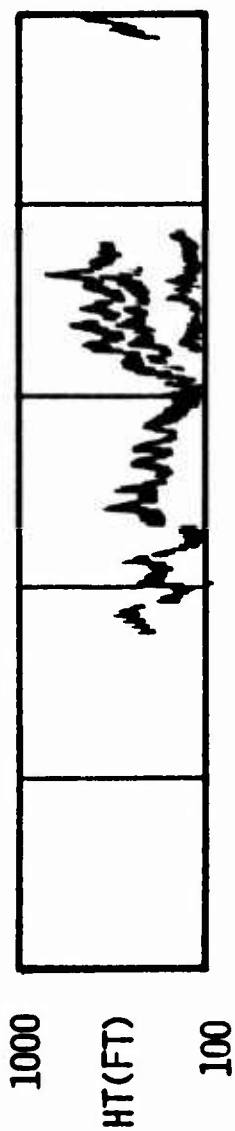
30

TIME (HST)
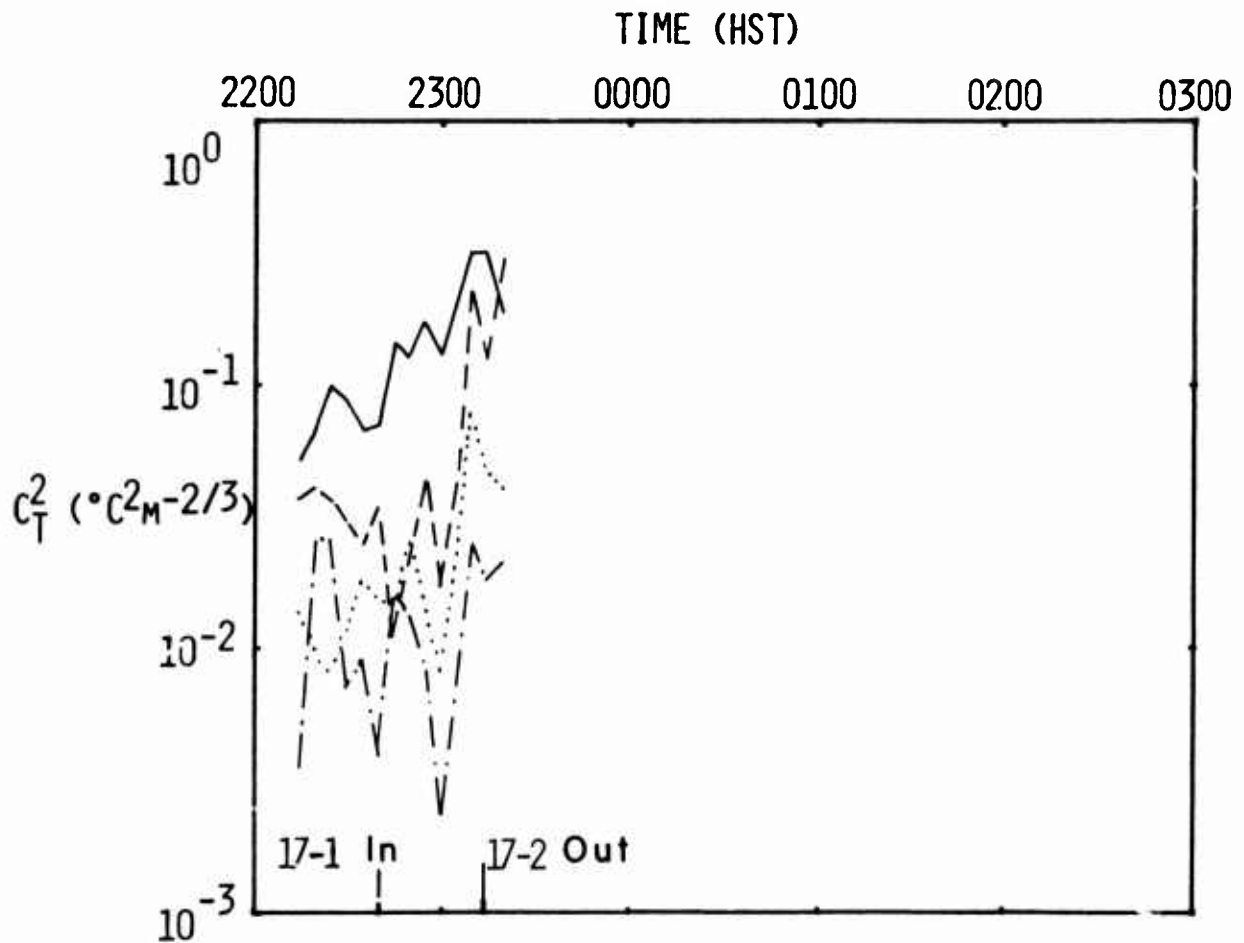
AMOS RUN 18

26 AUG 74

ACTIVE SENSORS 1-8

WS 1M/SEC

WD S

60" DOME NE

KEY (POSITION NO.)

——— POLE (1)

— — — TOP TOWER (4)

· · · · · · IN SLOT 60" (5)

— · — OUT SLOT 60" (6)

Figure 18

31

to characterizing the type of turbulent activity observed.

Shortly after sunset, a stable layer begins to develop over the mountain top. On windy nights, we observed strong sounder return over a substantial depth of the atmosphere above the surface. On calm nights, only a shallow inversion layer was observed. Regardless of surface wind conditions, gravity waves appeared and disappeared at levels throughout the sensing range of the sounder throughout much of each night. In general, all the features of the nighttime boundary layer observed over Mt. Haleakala are similar to those observed over any flat surface of the earth. The prime uncertainty we would express, based on the limited data presently available, is whether the depth of the boundary layer and the frequency of occurrence of windy and calm nights is also similar. Intuitively, one would expect a more shallow layer over the mountain peak on windy nights particu-larly, but more observations are required to permit analysis of this point.

Now, let us examine the plots of C_T^2 with reference to the acoustic sounder records. It is clear that regions of intense activity above the observatory are frequently decoupled from regions of intense activity in the immediate vicinity of the dome, particularly under light wind conditions. For example, the C_T^2 measurements near the dome showed large values only when the acoustic sounder also showed intense activity near the ground, not when the echoes were obtained from stratified layers

above the ground. Because of the strong decoupling that exists between these various layers at night, it is essential to determine seeing quality in some objective, quantitative manner at the same time the environmental observations are made.

E. Quantization in Terms of Seeing Degradation.

In the end, we will be comparing values of seeing degradation for all three sensors. The common parameter which we wish to use is Fried's coherence length r_0, defined for plane waves as

$$r_0 = \left\{ 0.423 \ k^2 \int_0^L C_n^2(z) \, dz \right\}^{-3/5}, \tag{4}$$

where k = wavenumber $(2\pi/\lambda)$

L = pathlength

and C_n^2 = refractive-index structure parameter.

If we can assume C_n^2 is constant over the region $0 \leq z \leq L$, then

$$r_0 = [0.423 k^2 L \ C_n^2]^{-3/5}. \tag{5}$$

Furthermore if we have a slab model for our propagation medium with C_n^2 constant in each slab, and if we calculate r_{0_i} for each slab labeled i=1,...,N, then we may sum the r_{0_i} in this manner:

$$r_0 = \left\{ \sum_{i=1}^N r_{0_i}^{5/3} \right\}^{-3/5}. \tag{6}$$

Values of C_n^2 are related to C_T^2 by

$$C_n^2 = (79.2 \times 10^{-6} p/T^2)^2 \, C_T^2 \qquad\qquad (7)$$

where p = pressure (mbar)

and   T = temperature (°K).

The constant 79.2×10^{-6}, in units of °K/mbar, is exact only for $\lambda = 0.5$ μm, in the middle of the visible, but varies little through the visible to infrared. Since the dependence of C_n^2 on p and T is so weak for the range of p and T to be encountered we typically took p=621 mbar and T=286°K, so that

$$C_n^2 = 3.6 \times 10^{-13} \, C_T^2, \quad (AMOS). \qquad\qquad (8)$$

Next we use r_0 in computing a value of the seeing angle β as λ/r_0. This corresponds to the Rayleigh resolution angle for diffraction-limited performance 1.22 λ/D, which we mentioned earlier. If we take β=1 arc sec as being sufficient to degrade imagery, then for visible wavelengths, r_0 = 0.11 m. In turn Eq. (4) says that $\int_0^L C_n^2(z)\,dz = 7.2 \times 10^{-13} \, m^{1/3}$. T. higgest dif-ficulty in interpreting this value for the microthermal probe data is in deciding upon the extent of the turbulence, L. Sup-pose we use the size of the dome, L=10 m. Then $C_n^2 = 7.2 \times 10^{-14} \, m^{-2/3}$ and after using Eq. (8), $C_T^2 = 0.20$ °$C^2 m^{-2/3}$. We may consider this to be a "critical" value of C_T^2 such that even if our C_T^2 data approaches 0.20 we say that dome turbulence is significantly affecting seeing. In fact, if we refer to Figs. 5-18, we see this occurs in Runs 3, 4 and 12, where the turbulence appears to be naturally generated by the atmosphere; in Run 14, after sun-up; and during Run 15 where the turbulence appears to be

34

generated by the dome shell. Since the values of C_T^2 do not exceed 0.20 for long periods of time, we may conclude that at times the turbulence generated by the domes is a degrading influence but not the consistently limiting factor.

We have computed values of r_0 for all runs and all fine-wire sensors and these are tabulated i· Table 3. This is perhaps the best place to judge the relative strengths of turbulence. We had to assume a value for L, so once again 10 m was taken. (We feel it is neither 3 nor 30 m. The dependence on L is $L^{-3/5}$, so if in the worst case the value of L is a factor of 3 off, then the r_0 would change by a factor of 1/2.) We have placed parentheses around values of r_0 inside the telescope tube, as the value of L_0 which we have used is not appropriate there. These values are indicative, however, of the low strength of turbulence we noted inside the tube.

We can see in Table 3 that r_0 is in the neighborhood of 0.1 to 0.2 m for a number of sensors during Runs 3, 4, 5, 6, 8, 10, 12, 14, 15 and 18. This indicates that the strength of local turbulence is often significant, but from these data we cannot tell if the source of turbulence is the dome structures. Since turbulence inside the 60" dome (Sensor 5) is consistently less than turbulence outside (Sensors 4 and 6) we can say that the turbulence is not coming from inside that dome. (Recall that a smaller r_0 indicates more turbulence and a greater degradation.) The opposite is true of the 48" dome, in that consistently there

35

TABLE 3

Values of r_0 (m) for microthermal probes assuming the extent of the turbulence L is 10 m. (If other values of L are of interest scale r_0 according to $L^{-3/5}$.)

Sensor	Run 3	Run 4	Run 5	Run 6
1,2	0.13	0.25	0.34	0.29
3	0.16	0.24	0.23	0.19
4	0.11	0.17	0.17	0.11
5	-	0.41	0.39	0.52
6	-	0.21	0.21	0.16
7	-	(0.37)	(0.56)	(0.60)
8	-	(0.58)	(0.81)	(0.84)
9	-	-	-	-
10	-	-	-	-

Sensor	Run 7	Run 8	Run 9	Run 10
1,2	0.51	0.21	missing	0.16
3	0.44	0.20	-	0.27
4	0.30	0.27	-	0.30
5	0.52	0.16	-	0.39
6	0.38	0.14	-	0.38
7	(0.70)	(0.47)	-	(0.80)
8	(1.05)	(0.38)	-	(0.82)
9	-	-	-	-
10	-	-	-	-

TABLE 3 (Continued)

Sensor	Run 11	Run 12	Run 13	Run 14
1,2	missing	0.16	0.33	0.10
3	-	0.21	0.45	0.13
4	-	0.16	0.64	0.16
5	-	0.30	0.56	missing
6	-	0.36	0.41	0.13
7	-	(1.17)	(1.02)	(0.80)
8	-	(0.93)	(1.68)	(0.32)
9	-	-	0.14	0.23
10	-	-	0.25	0.12

Sensor	Run 15	Run 16	Run 17	Run 18
1,2	0.70	0.49	0.25	0.13
3	0.51	0.35	0.26	0.34
4	0.32	0.23	0.27	0.20
5	0.11	0.24	0.79	0.40
6	0.08	0.21	0.24	0.56
7	(0.45)	(0.74)	(0.89)	(0.70)
8	(0.68)	(1.10)	(1.40)	(0.37)
9	0.21	0.26	-	-
10	0.39	0.46	-	-

Note: Values for sensors 7 and 8 are only indicative of low turbulence in that the assumption on the value of L_0 is undoubtably incorrect.

37

is more turbulence inside (Sensor 9) than outside (Sensor 10).
The 48" dome, unlike the 60", was in somewhat of an operational
state, even though some equipment was turned off.

III. ACOUSTIC SOUNDER CALIBRATED DATA

A. Background.

At the time the experiments were run at AMOS, the acoustic sounder had not undergone its final calibration. There was an additional unknown scale factor, hopefully a constant in altitude, which could only be determined by comparing the sounder output with values of C_T^2 measured by microthermal probes such as we described in the previous section. This calibration was effected by the AFCRL Boundary Layer Branch during a remote experiment at Jackass Flats Nevada during October 1974. The results of that experiment will be presented in a separate article to be published later by AFCRL, but we have the salient remarks here. In addition AFCRL is currently preparing a report covering the use of an acoustic sounder in relation to optical propagation through turbulence.[7]

B. Calibration Set-up.

Three pairs of fine wire platinum resistance thermometers, spaced one meter apart, were mounted at heights of 150, 290 and 440 ft on the BREN tower at the AEC Nevada Test Site at Jackass Flats. These sensors were sampled at a rate of 20 times a second and recorded on digital magnetic tape using AFCRL's computer-controlled data acquisition system.[8] Sounder signals were recorded on analog tape as they were for the AMOS experiments. The antenna was located far enough upwind to avoid

39

reflections from the tower. Since its beam width is roughly 45°, this meant a separation distance of 1500 ft from the tower. Sensors were not placed above 440 ft since the environment in Nevada is very dry and thus only noisy returns were sensed above about 500 ft.

C. Brief Remarks on Theory of Operation.

A recent report by Neff[9] contains a thorough treatment of the subject of acoustic sounders in measuring temperature fluctuations. The report has extensive references for those who are interested. The fundamental concepts are based on the fact that sharp discontinuities in the temperature or wind field will cause acoustic energy to be scattered or deflected from the propagation direction. In the backscatter direction (scattering angle of 180° from the propagation), the scattered energy is theoretically a function only of the temperature fluctuations. The theory also assumes that the scale size of the turbulent fluctuations causing the scatter is within the inertial subrange, thus providing a relationship between the backscatter cross-section and C_T^2, the temperature structure function.

D. Results of Calibration at Nevada.

To obtain statistically stable estimates of C_T^2 from the acoustic sounder and microthermal probes, we chose periods with fully developed convection when the turbulence is reasonably stationary and the atmospheric boundary layer is well mixed.

One-hour averages of C_T^2 were computed for each of the three heights.

Separate comparisons were made for each of the three heights to determine whether the derived calibration factors were invariant with height. Let us define a simple relation between the two values of C_T^2 measured as

$$C_{T\,(\text{Tower})}^2 = \alpha\, C_{T\,(\text{Sounder})}^2 . \tag{9}$$

The following values of α were obtained for unstable conditions:

$\alpha = 1.83$, for 150 ft altitude

$\alpha = 2.33$, for 290 ft altitude

and $\alpha = 2.89$, for 440 ft altitude.

Calibration factors for slightly stable cases characterized by light to moderate winds and good mixing were

$\alpha = 0.86$, for 150 ft altitude

$\alpha = 0.93$, for 290 ft altitude

and $\alpha = 1.03$, for 440 ft altitude.

The strong height dependence of the calibration factor α for unstable conditions, and the marked difference in α between convective (unstable) and stable conditions were unexpected and puzzling. The results suggest an unaccounted loss of acoustic energy that is apparently considerably more severe during unstable than stable conditions as well as the possibility of a

41

different scattering mechanism under stable conditions. Specula-
tion as to why the calibration factor varies is given in AFCRL's
report,[7] but there is not yet a conclusive explanation.

It should, of course, be noted that the immediate appli-
cation of the echo sounder at AMOS is for optical tracking prob-
lems under stable conditions for which results show only a weak
height dependence. This is, indeed, a fortuitous result for it
permits a quantitative analysis of the AMOS data on a rational
basis even though a full explanation of the scattering phenomena
is yet to be presented. For our purposes, we will use a value
of 1.00 for α.

E. Description of AMOS Data.

As already mentioned, all the AMOS experiments were con-
ducted under thermally stable conditions. The sounder was oper-
ated at a frequency of 2000 Hz; the pulse length selected was
50 msec; the delay time was set at 150 msec; and the pulse re-
petition rate was roughly 30 per minute. This gave a height
range of roughly 305 m (1000 feet). Surface measurements of
pressure, humidity, and temperature were obtained with a baro-
graph and a hygro-thermograph. Relative humidities were gener-
ally 40% or higher at all times, thus the increased effective
range with respect to Nevada. Lower relative humidities (10 -
20%) were observed only in the daytime during the course of these
experiments.

Values of C_T^2 were computed at 100 ft intervals from 150 to 950 ft for successive one-minute averaging periods. Rather than averaging over a 100 ft region (e.g. 100 to 200 ft), we have averaged only over an altitude band of approximately 50 ft. centered at the indicated levels. These values are tabulated for Runs 10-14 and 16-18 in the AFCRL report.[7] (Other runs were found to be too noisy.) Here we present averages for the entire run in Fig. 19 and in Table 4. Averaging times for these runs are the same as given in Table 2. Rather than to view plots of Fig. 19 as averages profiles, we prefer to think of them as the probability of locating a layer at a certain altitude, but in the units of C_T^2. Note there is an increasing probability of having a layer occur at altitudes near the top of the mountain rather than higher up. Indeed the rate of decay with altitude for the average overall runs (excluding Run 14 which extended through sun-up) is quite steep, in that it goes as $0.19z^{-1.37}$, with z in meters. This behavior was found by performing a least squares fit to the average profile and had a correlation coefficient "r" of 0.9929. In the boundary layer at night, under stable conditions, the dependence is $z^{-2/3}$; whereas during the day, in convective unstable conditions, the dependence is $z^{-4/3}$. This suggests that the presence of the mountain has an influence on the stratification of the turbulence. We further suppose that the region of 100 to 1000 ft above the mountaintop is not necessarily indicative of what occurs above 1000 ft. That is, one should not take the $z^{-1.37}$ profile too seriously outside the measurement range.

43
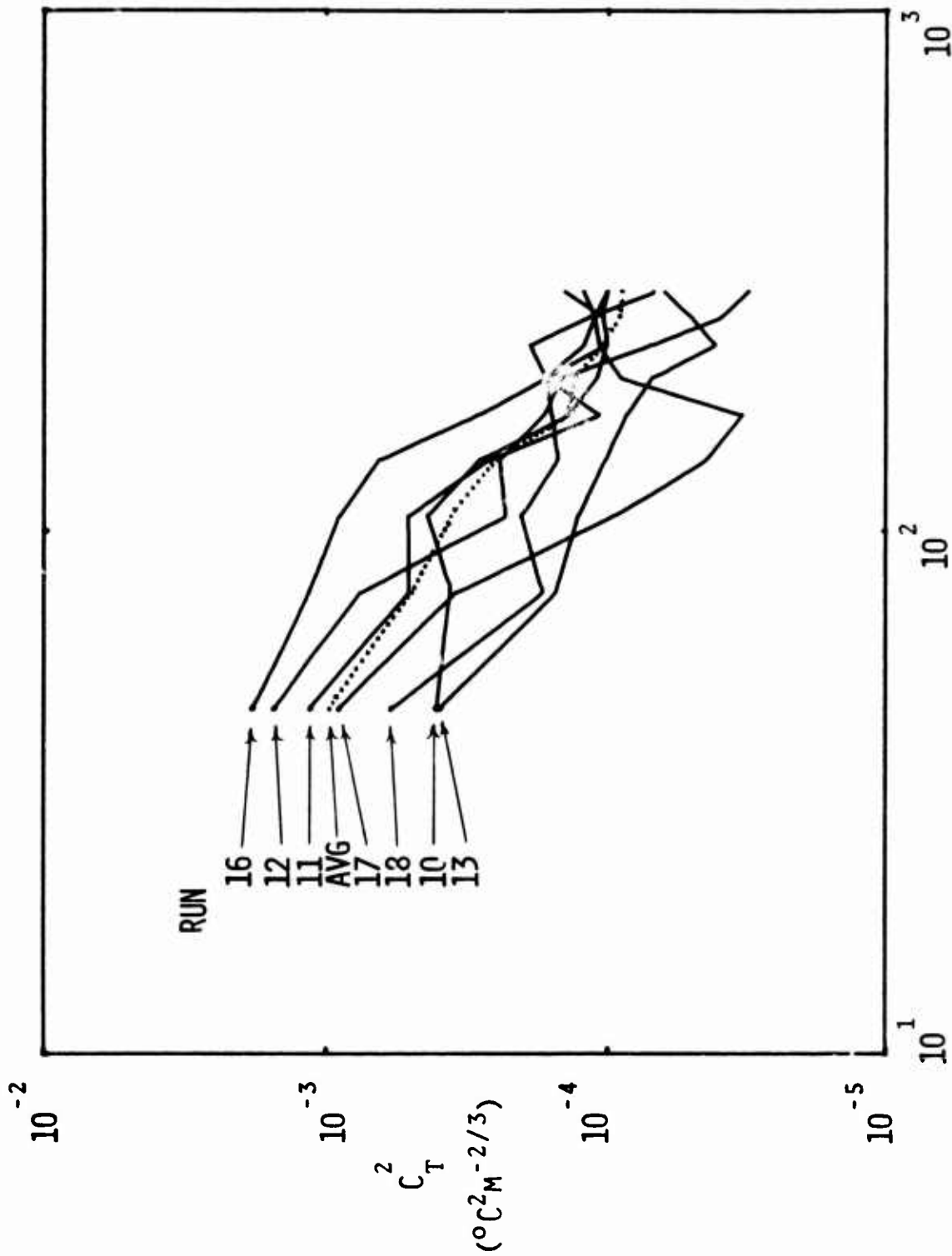
ALTITUDE ABOVE SITE z(m)

Figure 19. Profiles of Turbulence for Runs 10-13 and 15-18 as sensed by the acoustic sounder. Also shown is the average of these profiles.

TABLE 4

Values of integrated C_n^2 and coherence length r_0 for the acoustic sounder profiles.

Run	$\int C_n^2\ dz\ (m^{-1/3})$	r_0 (m)
10	2.20×10^{-14}	0.89
11	3.34×10^{-14}	0.69
12	3.53×10^{-14}	0.67
13	1.18×10^{-14}	1.29
14	2.87×10^{-14}	0.76
16	5.83×10^{-14}	0.50
17	2.02×10^{-14}	0.94
18	1.91×10^{-14}	0.97
Avg	2.86×10^{-14}	0.76

IV. OPTICAL MEASUREMENTS

A. Experimental Technique.

It was essential for the experiment to include one in-
strument which provided an integrated measure of turbulence for
the entire atmosphere. The instrument should measure optical
phase, or phase-related quantity such as arrival angle. Ampli-
tude scintillation is not sufficient because that is affected
more by high altitude turbulence and hardly affected by low al-
titude turbulence at all. The most reliable measurement is of
arrival angle difference, which is not affected by telescope
tracking errors. An analysis of this measurement is provided by
Fried.[10]

The instrument itself must be portable and be capable of
providing short exposure, quantitative results. Portability is
required so that seeing conditions as viewed from inside and
outside the dome can be investigated. The data must be of short
exposure (less than roughly the 25 msec time constant of the
atmosphere) so that the fluctuations in arrival angle do not
cause a blur in the recorded data. Obviously quantitative data
are required so that comparisons with other instruments can be
made. Hence we have avoided subjective measures such as were
done in the original site survey.

The measurements were made on a small telescope which had
fitted over the aperture a Hartmann mask consisting of two holes.

To measure arrival angle at the individual subapertures, the telescope was pointed at a bright star, and the images of the star for the two subapertures were recorded on film. To achieve sufficient separation of the images on the film, the telescope was slightly defocused. We describe the procedure analytically in Appendix A.

B. Instrument.

The instrument chosen for use in this experiment was a Questar Seven. This telescope is a Maksutov Cassegrain Catadioptric system with a clear aperture of 7 inches, obscuration ratio of 0.34 and a prime focal length of approximately 112 inches. In order to increase the image motion a minus 66.06 mm FL Barlow Lens was used to provide a 2X magnification. An assortment of Questar accessories was also used in order to obtain a fully portable instrument capable of sidereal tracking. A schematic diagram of the device is in Fig. 20.

Data recording was accomplished by use of a Questar-modified Nikon F 35mm camera body. This camera was equipped with a 250 exposure motorized film drive. However, film advancement and shutter release were performed manually in order to avoid excessive vibration. Kodak RAR 2484 film was used to record the images. Processing was carried out for two minutes at 94°F in D-19 developer.

Two Hartmann plates were constructed from extra lens

47
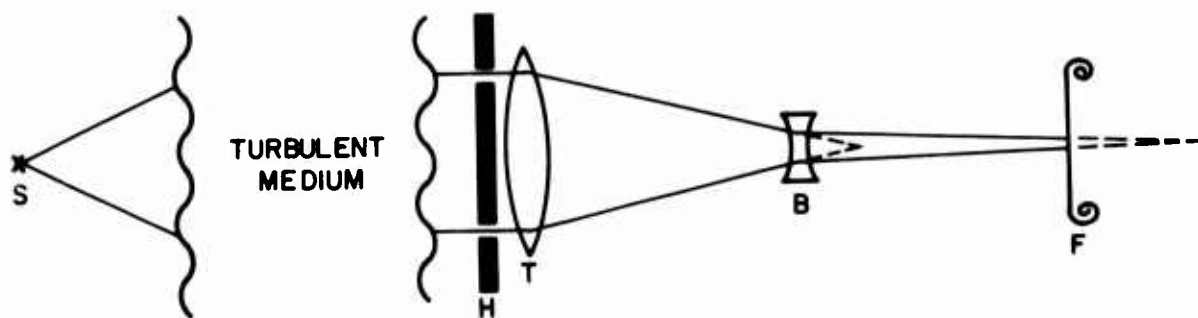
Figure 20.   Schematic Diagram of Optical System Showing Source
S, Telescope T, Hartmann Plate H, Barlow Lens B,
and Film F.

caps. One contained three 2.25 inch diameter holes at two different spacings. At times this mask had one of the three holes covered. The second contained six 1.0 inch holes at five different spacings.

C. Measurements.

Data were collected at AMOS during the period 19 August to 31 August 1974. A summary of all data runs attempted is given in Table 5. In all, data were taken at three different locations: inside the east dome of the observatory, in the aircraft spotters enclosure approximately fifty feet north of the observatory and on top of Red Hill (highest point on the mountain). These locations are indicated in Figs. 1 and 2. Of the twenty-eight data runs attempted, two were exposure sequences, two were taken with the 1.0 inch aperture plate and twenty-four were taken with the 2.25 inch aperture plate. Of these last twenty-four, five produced no data due to camera malfunction or excessive vibration. Thus there is potentially good data from nineteen runs with this plate.

These data can potentially result in information relative to the following:

    1. Comparative seeing inside and outside of the dome.

    2. Comparative seeing inside the dome and at Red Hill.

    3. Correlation with the acoustic and microthermal data.

    4. Comparative seeing inside the dome with different angles between the dome slot and the wind direction.

49

TABLE 5. OPTICAL DATA SUMMARY

Date Time	Data ID	Location[1]	Hartmann[2] Plate	Object; θ EL	Comments
8/22 0030	ESNB	Outside	2	Vega	Exposure sequence
8/23 0030	8-1	Outside	1,3	Vega	Exposure sequence and 25 frames of Hartmann data
8/23 2200	-	Outside	1	Vega	No data: vibration in motor drive
8/23 2300	-	Outside	1	Vega	No data: vibration in motor drive
8/24 0100	-	Outside	1	Altair	No data: camera malfunction
8/24 2200	13-1	Outside	1	Vega, 67°	Acoustic and microthermal data
8/24 2300	13-2	Outside	1	Altair, 75°	Acoustic and microthermal data
8/24 2330	13-3	Outside	1	Altair, 68°	Acoustic and microthermal data
8/25 0015	13-4	Outside	1	Altair, 58°	Acoustic and microthermal data
8/25 2145	15-1	Outside	1	Vega, 65°	Acoustic and microthermal data partial data loss due to power failure during development
8/25 2230	15-2	Inside	1	Vega, 58°	Acoustic and microthermal data
8/26 0000	16-1	Inside	1	Altair, 55°	Acoustic and microthermal data only 70 frames due to wrong focus
8/26 0030	16-2	Outside	1	Altair, 48°	Acoustic and microthermal data
8/26 2010	16-3	Outside	3	Vega, 72°	Acoustic and microthermal data
8/26 2045	-	Outside	1	Vega, 72°	No data: camera malfunction
8/26 2130	-	Inside	1	Vega, 70°	No data: camera malfunction
8/26 2240	17-1	Inside	1	Vega, 60°	Acoustic and microthermal data only ≈ 90 frames
8/26 2315	17-2	Outside	1	Vega, 54°	Acoustic and microthermal data

TABLE 5. (cont'd)

Date Time	Data ID	Location[1]	Hartmann[2] Plate	Object; θ EL	Comments
8/27 2100	19-1	Outside	2	Vega, 72°	One Hartmann aperture blocked
8/27 2130	19-2	Inside	2	Vega, 69°	Further activity suspended due to power failure
8/29 2030	20-1	Inside	2	Vega, 72°	Wind ≈ 45° off slot
8/29 2130	20-2	Inside	2	Vega, 68°	Wind ≈ 135° off slot
8/29 2200	20-3	Inside	2	Altair, 78°	Slot down wind
8/29 2215	20-4	Inside	2	Altair, 75°	Slot up wind
8/30 2045	21-1	Red Hill	2	Vega, 72°	Outside visitors center, not in wind shadow
8/30 2130	21-2	Red Hill	2	Vega, 68°	Same location as case 21-1
8/30 2245	21-3	Inside	2	Altair, 78°	
8/30 2300	21-4	Inside	3	Altair, 75°	

Notes: (1) Outside: Aircraft spotters enclosure except for case ESNB.
Inside: East dome (60" dome).
Red Hill: Highest point on mountain.

(2) Hartmann plates:
1 - three 2.25" apertures
2 - same as 1 with one hole blocked
3 - six 1.0" apertures

(3) Each data run (except exposure seq.) consists of ≈ 120 frames
of data. Exposure time = 1/60 sec. for plates 1 and 2; 1/30
sec. for 3.

5. Effect of Hartmann aperture spacing.

6. Temporal variation in seeing.

D. Data Processing.

Initial data reduction was carried out using the David
Mann Optical Comparator. This is a device which uses precision
lead screws to position cross hairs on the desired location.
Readout is automatic on IBM cards and a typewriter. Experienced
operators working with well defined circular images (diameter
~ 10 μm) quote measurements with a repeatability of less than
three microns.

In order to determine the repeatability on our data, ten
2.25 inch Hartmann frames taken on August 23 (Run 8-1) were se-
lected at random and read by two different operators. The pro-
cedure used was to visually estimate the center of one image and
zero the readout. The center of a second image was then visually
estimated and a reading recorded (displacement in two orthogonal
directions). This procedure was repeated ten times on each frame
by each operator.

The resulting data was first reduced for linear spacing.
Averaged (smoothed) spacings and ten reading variances were then
calculated for each frame. Finally, the ten frame averages and
variances (of the smoothed values) were calculated. The results
of this analysis are given in Table 6. As can be seen, the two
sets of smoothed values are within one sigma (larger value) in

52

TABLE 6. SAMPLE DATA REDUCTION

	Separation (μm)		Standard Deviation (μm)	
	Operator 1	Operator 2	Operator 1	Operator 2
Single Frame No.				
1	348	349	1.9	6.5
2	358	355	4.3	4.4
3	336	331	6.1	3.4
4	335	350	6.2	3.4
5	353	354	4.1	5.4
6	294	298	3.7	5.6
7	375	380	3.7	7.2
8	334	328	4.7	6.4
9	333	326	3.8	6.0
10	318	317	3.3	4.0
Ten Frame Average	338.3	338.8	22.3	22.1

all cases except frame nine which has a slightly larger difference. Assuming the measurements are independent with Gaussian random read errors, the estimated sigma (due to read errors) associated with the ten frame averaged spacing should be of order 0.5 µm. The estimated sigma associated with the ten frame root variance should be of order 0.4 and 0.8 µm for the two operators, respectively. It should be noted that this analysis does not deal exactly with the quantization error (±1 µm) in the readout. However, the turbulence induced variances are expected to be larger than 1 µm (as indicated in Table 6) and so this effect should not be significant.

A second check on errors was obtained by processing the same twenty-six frame data set on two different days (same operator). Five independent readings of each frame were made. The average spacings were 203.0 µm and 204.8 µm respectively. The standard deviations were 18.4 µm and 17.6 µm, respectively. These values are consistent with the errors indicated by the data of Table 6.

Based on these results, it appears that this technique should result in an accurate data reduction. The number of repeated readings on a single frame has been set at five. When combined with other parameters (number of frames processed ≈ 100, expected levels of variances, etc.), we expect that a ±10% measurement of the turbulence induced variation in spacing should be obtained.

E. Results.

In all twenty data sets were reduced. The results, given in Table 7, are for seven nights over a span of nine days.

The image pair reduced had a 4.75 inch nominal aperture plane spacing, $(V_1 - V_2)$. As can be seen, these sets consist of three subsets in which data were collected inside and outside the observatory within a short period ($\leq$45 minutes). Preliminary estimates of the errors indicate that the first five cases are accurate to better than ±10% (i.e., "standard deviation" of the standard deviation). However for data set 17-2, an excessive amount of defocus was used leading to large, under-exposed images that were more difficult to read. Therefore, errors may be somewhat higher than ±10% for this case.

The values of (Δ/f) were calculated from Eq. (A.4) using the measured mean values. Due to the smallness of this factor in all cases, its effect was ignored when calculating the angle of arrival via Eq. (A.5). A value of 224 inch was used for the focal length. The correlation scale, r_0, was calculated from Eqs. (A.7-A.9) assuming a coefficient of one half in Eq. (A.9) and a wavelength of 0.5 μm. In addition, it was assumed that no correlation existed between the two apertures. The theoretical model of Fried[11] yields approximately the same results.

As can be seen, only one subset (15-1 and 15-2) of data indicates a major difference in angle of arrival variance inside

TABLE 7. DIFFERENTIAL ANGLE OF ARRIVAL MEASUREMENTS

Run	Date; Time	Location; $\theta_{EL}°$	N	$\bar{r}$ (μm)	$\bar{v}^{1/2}$ (μm)	$(\Delta/R) \times 10^{-3}$	$\langle(\alpha_1-\alpha_2)^2\rangle^{1/2}$ (μrad)	Derived r_0 (cm)	Corrected r_0 (cm)
8-1	8/22; 2340	Outside; ≈50	10	338	21	2.8	3.7	8.5	10.0
13-1	8/24; 2200	Outside; 67	49	442	26	3.7	4.5	6.8	7.2
13-2	8/24; 2300	Outside; 75	50	311	30	2.6	5.2	5.7	5.8
13-3	8/24; 2330	Outside; 68	50	297	21	2.5	3.7	8.5	8.9
13-4	8/25; 0015	Outside; 58	50	263	24	2.2	4.3	7.2	7.9
15-1	8/25; 2145	Outside; 65	72	372	33	3.1	5.8	5.0	5.3
15-2	8/25; 2230	Inside; 58	99	331	52	2.7	9.1	2.6	2.9
16-1	8/26; 0000	Inside; 55	79	270	41	2.2	7.2	3.8	4.3
16-2	8/26; 0030	Outside; 48	98	524	46	4.3	8.1	3.3	3.9
17-1	8/26; 2045	Inside; 60	79	210	22	1.7	3.9	8.1	8.8
17-2	8/26; 2130	Outside; 54	89	1192	28	4.4	4.9	6.1	6.9
19-1	8/27; 2100	Outside; 72	50	348	21	2.9	3.7	8.5	8.8
19-2	8/27; 2130	Inside; 68	49	309	18	2.6	3.2	10.3	10.8
20-1	8/29; 2030	Inside; 72	50	160	11	1.3	2.0	17.8	18.3
20-2	8/29; 2130	Inside; 68	50	140	12	1.2	2.1	16.7	17.5
20-3	8/29; 2200	Inside; 78	50	109	12	0.9	2.1	16.7	16.9
20-4	8/29; 2215	Inside; 75	50	89	13	0.7	2.3	15.2	15.5
21-1	8/30; 2C45	Red Hill; 72	50	350	15	2.9	2.7	12.6	13.0
21-2	8/30; 2130	Red Hill; 68	50	378	14	3.1	2.5	13.9	14.5
21-3	8/30; 2245	Inside; 78	50	192	12	1.6	2.1	16.7	16.9

and outside the observatory. Based on the estimated 10% variance in the measurement of the sample variance (σ_r), the difference represents roughly a four sigma change. The other two subsets have differences which are less than approximately one sigma and therefore cannot be considered statistically significant.

A rather surprising result is the small calculated values of r_0. Seeing is thought to be typically 1 arc sec which corresponds to an r_0 of approximately 11 cm. The data taken on the night of August 25 implies seeing angles as large as 4 arc sec. Such values are not unreasonable, particularly in view of the fact that on the next night (8/26) the values of r_0 were much closer to 11 cm. As the experiment continued, values of r_0 increased, and this emphasizes the fact that this recording period may not be representative of year-round conditions at AMOS. Note also that microthermal and sounder measurements had ceased on 26 August, just before the seeing improved. All of the derived r_0 values are plotted in Fig. 21 to further demonstrate the non-stationarity of this parameter.

All data were collected on stars well away from zenith. Theory[12] predicts a $(\sin \theta_{EL})^{3/5}$ dependence for r_0 leading to smaller values at large zenith angles. For example, making this correction to case 17-1 yields an r_0 of 8.8 cm which corresponds approximately to vertical seeing angle ($\sim\lambda/r_0$) of 1.2 arc sec. We have provided values of r_0 corrected by this zenith angle

57

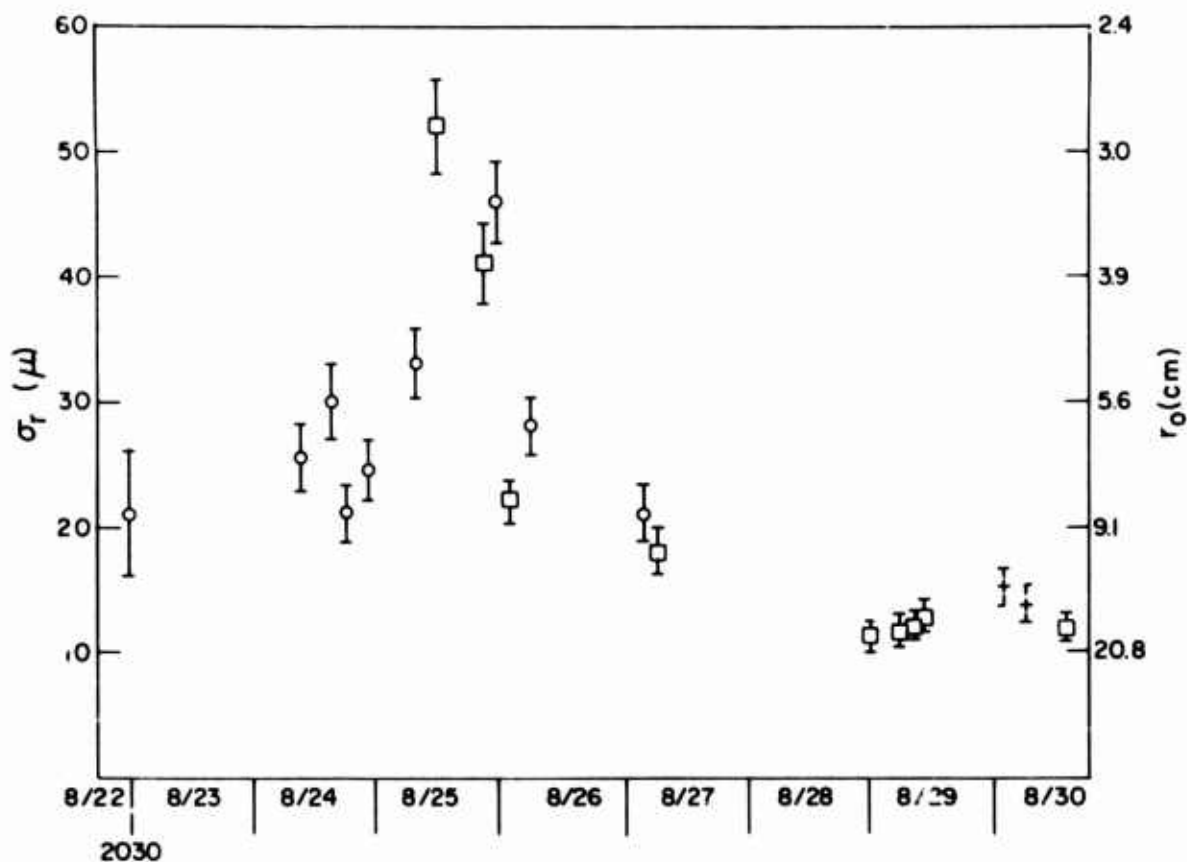Figure 21. Measured Differential Angle of Arrival Standard Deviations and Derived Values of r_0. Locations of data collection are: O, outside observatory; □ , inside observatory; +, atop Red Hill. The bars indicated the estimated one σ spread in the data due to finite sample size.

58

dependence in Table 7 as a further reference. Now the values of r_0 range from 2.9 to 18.3 cm with a mean of 10.2 cm.

V. CONCLUSIONS

A. Comparison of All Data

Within each of the previous sections we concluded with a table of r_0 values for the runs in which good data were collected. Now we will compare those values for the times when all three experiments were in operation, and will include the two runs where only acoustic sounder data are missing. Furthermore we shall consider the percentage contribution of the regions sensed by the acoustic and fine-wire probes to the total turbulence as sensed by the Hartmann device.

Consider Table 8. The microthermal sensors gave us values of r_0 ranging from 0.21 to 0.70 m in these runs. Although we used sensor 1, which was positioned well away from the dome and 4 m above ground, the values change little if we used sensor 4, on top the tower displaced 3 m from the dome, or sensor 6, mounted just outside the dome slot. Basically these sensors contribute a noticeable but small percentage to the overall. We may just say that these values of r_0 can in the worst cases be a degrading influence on overall seeing. Recall that in Table 3, where we surveyed all the runs, some r_0 were as low as 0.11 m. Thus on occasion the turbulence in the vicinity of the dome is a limiting factor. The important fact which we cannot derive conclusively from these data is whether the turbulence is actually coming from the buildings. Only during Runs

60

TABLE 8

COMPARISON OF VALUES OF r_O (m) AND PERCENT CONTRIBUTION TO THE TOTAL r_O FOR ALL INSTRUMENTS WHEN ALL INSTRUMENTS WERE OPERATING SIMULTANEOUSLY

RUN	SENSOR 1 r_O , %	ACOUSTIC r_O , %	OPTICAL r_O (100%)	MISSING %
8-1	0.21 , 29	missing	0.10	71
13-1	0.33 , 8	1.29 , 1	0.072	91
13-2	0.33 , 6	1.29 , 1/2	0.058	93.5
13-3	0.33 , 11	1.29 , 1	0.089	88
13-4	0.33 , 9	1.29 , 1	0.079	90
15-1	0.70 , 1	missing	0.053	99
15-2	0.70 , 1/2	missing	0.029	99.5
16-1	0.49 , 2	0.50 , 2	0.043	96
16-2	0.49 , 2	0.50 , 1	0.039	97
17-1*	0.24 , 19	0.95 , 2	0.088	79
17-2*	0.24 , 13	0.95 , 1	0.069	86

*Used average of Runs 17 and 18 for sensor 1, as optical measurements were made between these runs.

15 and 16 does it appear that ambient turbulence is low (Sensors 1 and 3), but turbulence sensed by Sensors 4, 5 and 6 is quite strong.

The acoustic sounder data are more clear-cut. Values of r_0 for the region of 100 to 1000 ft above the site are much too large to be a limiting factor, or even a contributing one.

The Hartmann device, in principle, should have indicated an improvement in seeing when it was moved from inside to outside the dome. That occured only in one case, Runs 15-1 and 15-2, but in Runs 19-1 and 19-2 conditions *improved* by moving inside. Furthermore, the other runs showed no noticeable improvement or degradation incurred by moving the instrument outside. This further suggests that turbulence in the vicinity of the dome may be roughly a 10-30% contribution and hardly a constant in time.

According to Table 8, there is from 71 to 99.5% of the turbulence which was not sensed by the sounder or the fine-wire probes. This turbulence must be in the regions of 60 to 100 ft and above 1000 ft. We are inclined to think that the unaccounted turbulence is well above 1000 ft and may be associated with strong temperature inversions, such as at the tropopause.

The situation is slightly different at the 48" dome than at the 60" dome. Consistently we noted as much or more turbulence inside as outside the 48" dome; whereas the reverse was

true at the 60" dome. This would suggest a thermal contamination problem in the 48" dome, caused perhaps by heat exchangers, power supplies, etc. Either these might be removed or the heat so generated be vented downwind of the dome.

B. Summary of Conclusions.

We have tabulated all our conclusions with respect to seeing degradation and its causes at AMOS in the following list for convenience.

(1) The region of 100 to 1000 ft altitude does not have significant strengths of turbulence to degrade seeing.

(2) The turbulence in the vicinity of the dome structures can on occasion be a significant factor, but typically is only a 10-30% contribution to total seeing degradation.

(3) Local turbulence appears to be naturally generated in most instances, although in certain runs significant turbulence appeared to peel from the dome structures.

(4) Additional seeing degradation is caused by turbulence generated within the 48" dome when it is in roughly an operational configuration. The same would probably be true for the 60" dome were it operational.

(5) Significant turbulence must lie between 60 and 100 ft and above 1000 ft altitude, and may be centralized at temperature inversions such as the tropopause.

C. Recommendations and Future Work.

Any scheme which would reduce heat absorption on the outer surfaces would improve seeing a noticeable amount. This might include special paint, and venting and cooling of the outer wall. The inner walls stay cool and thus air conditioning is not required. The heat-generating equipment in the 48" dome should either be cooled in place or should be moved. This equipment will still generate heat no matter where it is, and one should be careful in positioning heat exchangers and vent ducts. The dome doors should be pointed away from the sun in the afternoon. This will not improve seeing when looking downwind but may improve it looking upwind.

A routine micrometeorological station is being set up at AMOS to do the measurements we discussed, excluding the Hartmann Test, continuously. The system involves two towers, one north and one south of the domes. On each tower will be three fine-wire sensors and a wind set (speed and direction). Also a thermometer will provide a continuous record of temperature. The acoustic sounder will be permanently installed as well. All the signals will be processed in real time by an on-site mini-computer which will identify the quality of seeing and will tell the operator when a sensor is not working properly. This system will ultimately satisfy a major objection to the August 1974 experiment, that it was of too short duration.

A series of ancillary experiments will be conducted

during 1975-76 which will provide further information on the seeing at AMOS. This includes two instruments which measure the atmospheric Optical Transfer Function (OTF) and thus r_0 directly: the Hughes Research Lab Seeing Monitor (SM) and the ITEK Real Time Atmospheric Measurements System (RTAM). These instruments will be run simultaneously with the Hartmann device to mutually verify their outputs. An additional instrument being procured from NOAA measures the scintillation covariance function and provides a crude profile of turbulence. This will demonstrate whether the turbulence which appears to be at high altitudes really is at those heights. Other experiments to be run include rawinsonde launches from the top of Mt. Haleakala (to get a better picture of the wind and temperature in the immediate vicinity of the site) and aircraft flights with fine-wire probes (to measure C_T^2 versus altitude for the first 7000 ft above AMOS).

Data from all of these measurements will then be combined to form a phenomenological turbulence model of AMOS. The objective is to provide data for the design of a compensated imaging system and data on seeing quality for routine site operation. Without a doubt this is the most intensive set of measurements ever performed on an observatory with the sole purpose of quantifying and improving seeing conditions.

65

APPENDIX A

THEORY RELATING HARTMANN TESTING TO SEEING VALUES

Consider a wave propagating from a distant point source, through the atmosphere to the image plane of a telescope. The image plane intensity is given by

$$I_I(\tilde{x}) \sim \left| \int d\tilde{v} \, W(\tilde{v}) \, A(\tilde{v}) \, \exp\left\{ \frac{-ik}{R} \, \tilde{x} \cdot \tilde{v} + i\phi_A(\tilde{v}) \right\} \right|^2, \qquad (A.1)$$

where $W(\tilde{v})$ is the aperture pupil function (assumed real) and $A(\tilde{v})$ and $\phi(\tilde{v})$ are the aperture plane amplitude and phase distortion generated by the atmosphere. The symbol k is the wave number, and R is the focal length of the telescope. Provided the telescope aperture (D) is small with respect to the characteristic scale of the phase fluctuations (Λ_ϕ), $\phi_A(\tilde{v})$ can be approximated by the first two terms in a Taylor series expansion yielding

$$I_I(\tilde{x}) \sim \left| \int d\tilde{v} \, W(\tilde{v}) \, A(\tilde{v}) \, \exp\left\{ -ik \left[\frac{\tilde{x}}{R} - \left[\frac{\tilde{\nabla}\phi_A(o)}{k} \right] \right] \cdot \tilde{v} \right\} \right|^2, \quad (A.2)$$

where $\tilde{\nabla}\phi_A(o)$ is the spatial derivative of the atmospheric phase evaluated at the center of the aperture. Equation (A.2) indicated that the image plane intensity is just a distorted Airy pattern (due to A) with center at

$$\tilde{x}_c = \frac{R}{k} \, \tilde{\nabla}\phi_A(o) = \tilde{\alpha} R \qquad (A.3)$$

where $\tilde{\alpha}$ is the angle of arrival, i.e., the angle between the

66

true and apparent direction of the star (as judged by the center of the image). Thus by observing the motion of the image of a star through a telescope of small aperture, these data can be reduced for the atmospheric angle of arrival fluctuations.

However, there is at least one difficulty with tracking the motion of a single star image. The position of the image also depends on telescope tracking and wind loading which cannot be separated from turbulence effects. Assuming that these two effects cause motion of the telescope as a whole, a convenient way of separating turbulence and tracking effects is to use two stars and reduce for the differential motion between the two images.

This same objective can be achieved with a single star by use of a telescope fitted with an aperture mask with two or more holes. By defocusing the image, a Fresnel image of the mask will be formed. This technique is basically a classical Hartmann test except that instead of processing a single frame of data, a series of short exposure images is processed for the required statistical information.

Modifying the above analysis to the case of a two hole Hartmann plate leads to a time averaged image position difference of

$$\langle x_1 - x_2 \rangle = (\Delta/f)(V_1 - V_2), \tag{A.4}$$

where f is the telescope focal length, Δ is the amount of defocus

67

and $(V_1 - V_2)$ is the separation of the Hartmann hole centers. The variance in the differential angle of arrival (one dimensional) is

$$\langle (\alpha_1 - \alpha_2)^2 \rangle = \frac{\langle (x_1 - x_2)^2 \rangle - \langle x_1 - x_2 \rangle^2}{f^2 (1 - \Delta/f)^2} . \qquad \text{(A.5)}$$

Equation (A.5) shows that provided (Δ/f) is small, the amount of defocus used is not critical for a measurement of the angle of arrival variance. However it is important for establishing sensor requirements since it affects the energy density of the Hartmann images. The angular difference is related to the single aperture angle of arrival of Eq. (A.3) by

$$\langle (\alpha_1 - \alpha_2)^2 \rangle = \langle \alpha^2 \rangle \, C_{12} , \qquad \text{(A.6)}$$

where C_{12} accounts for any correlation between the two Hartmann apertures. Theoretical values of C_{12} have recently been calculated by Fried.[11]

Angle of arrival measurements can also fulfill the requirement of allowing extrapolation to large diameter apertures. For a small aperture instrument, it can be shown that[12] the squared variance of the angle of arrival (one component) is given by

$$\langle \alpha^2 \rangle = \frac{D_\phi(d)}{k^2 \, d^2} , \qquad \text{(A.7)}$$

where d is the aperture diameter and D_ϕ is the phase structure function defined by $\langle (\phi(x) - \phi(x+d))^2 \rangle$. The long exposure

68

optical transfer function for an aperture of arbitrary size is given by[13]

$$\langle \tau(f) \rangle = \tau_0(\lambda R f) \, e^{-\frac{1}{2} \left[D_\ell(\lambda R f) + D_\phi(\lambda R f) \right]}, \qquad (A.8)$$

where D_ℓ is the atmospheric log-amplitude structure function and $\tau_0(\lambda R f)$ is the lens (no atmosphere) MTF. It is usually this quantity that is used to specify classical resolution.

Assuming a Kolmogorov turbulence spectrum and the Rytov approximation,[13]

$$D(\rho) = D_\ell(\rho) + D_\phi(\rho) = 6.88(\rho/r_0)^{5/3} \begin{Bmatrix} 1/2 & \text{for } \rho \ll \sqrt{\lambda L} \\ 1 & \text{for } \rho \gg \sqrt{\lambda L} \end{Bmatrix}, \quad (A.9)$$

provided ρ is larger than some small number (of order one millimeter or smaller). The symbol L is the pathlength through turbulence. Provided the model assumed is correct, the parameter r_0 controls the shape of the long exposure MTF and hence classical resolution and seeing. From Eqs. (A.7) and (A.9) it can be seen that the angle of arrival variance can be used to determine r_0, at least to within a factor of $2^{-3/5}$. Thus from a measurement of $\langle \alpha^2 \rangle$, a minimum value of r_0, and hence a minimum resolution for a large aperture instrument can be implied.

REFERENCES

[1] R. Zirkind, *Appl. Opt.* 4, 1077 (1965).

[2,3] (These references will be made available to qualified military or government request from RADC(OCSE), Griffiss AFB NY 13441.

[4] D. P. Greenwood and D. O. Tarazano, *A Proposed Form for the Atmospheric Microtemperature Spatial Spectrum in the Input Range*, RADC-TR-74-19, Griffiss AFB NY (1974). (AD776 294)

[5] D. P. Greenwood and D. B. Youmans, *A Fine-Wire Microtemperature Probe for Atmospheric Turbulence Measurements*, RADC Technical Report, Griffiss AFB NY (1975). (RADC-TR-75-240)

[6] F. F. Hall, Jr., *Temperature and Wind Structure Studies by Acoustic Echo Sounding*, Ch 18 in *Remote Sensing of the Troposphere*, ed. by V. E. Derr (US Govt Printing Office #0323-0011, 1972).

[7] D. A. Haugen, J. C. Kaimal and J. T. Newman, *The Use of an / oustic Echo Sounder for Optical Tracking Application*, AFCRL Technical Report, Hanscom AFB MA (1975).

[8] J. C. Kaimal, D. A. Haugen and J. T. Newman, *J. Appl. Meteorol.* 5, 411 (1966).

[9] W. D. Neff, *Quantitative Evaluation of Acoustic Echoes from the Planetary Boundary Layer*, NOAA Tech Report ERL 322-WPL-38, Boulder CO (1975).

[10] D. L. Fried, *Rad. Sci.* 10, 71 (1975).

[11] D. L. Fried, *Theoretical Study of Non Standard Imaging Concepts*, RADC-TR-74-185 (May 1974). (AD783 276)

[12] R. S. Lawrence and J. W. Strohbehn, *Proc. IEEE* 58, 1523 (1970).

[13] D. L. Fried, *J. Opt. Soc. Am.* 56, 1372 (1966).